Supplementary Document: The Role of Connectivity in Understanding Grassland-Shrubland Regime Shifts: Impacts of Aridity, Grazing, and Wind Dynamics

Keywords: Land Degradation; Grass-Shrub Dynamics; State Change; Complex Networks; Multilayer Network

Authorship: Shubham Tiwari[*1], Laura Turnbull[1] and John Wainwright[1]

[*]: Corresponding Author

[1]: Department of Geography, Durham University, Durham, United Kingdom

Contents

S1 Scope of the Supplementary File

This file provides methodological detail and complete numerical outputs that could not be included in the main manuscript. It is organised to enable readers to (i) reproduce the simulations and (ii) verify every statement in the Results section of the main manuscript, while avoiding narrative repetition. All figures in this file are labelled with an "S" prefix (e.g., Figure S1) to distinguish them from those in the main text.

S2 Extended Methods

S2.1 Model amendments relative to Stewart et al. (2014)

S2.1 Dynamic nitrogen-redistribution weights: In the original model, lateral nitrogen transport is controlled using fixed weights: 45% (water), 45% (wind), and 10% (grazers). To account for interannual rainfall variability, we introduced a linear rainfall-scaling factor defined for year *x* as:

$$\mathrm{f(x)} = (\mathrm{rain_x} - \mathrm{rain}_{avg})/\mathrm{rain}_{avg}.$$

The annual redistribution matrix for nitrogen ($\mathrm{N_x}$) is then calculated as:

$$\mathrm{N_x} = 0.45(1+\mathrm{f(x)}) \times \mathrm{S_{water}} \times \mathrm{N_{total}} + 0.45(1-\mathrm{f(x)}) \times \mathrm{S_{wind}} \times \mathrm{N_{total}} + 0.1 \times \mathrm{S_{animal}} \times \mathrm{N_{total}}$$

where S represents the "smoosh" matrices proposed by Stewart et al. (2014) and $\mathrm{N_{total}}$ is the nitrogen pool available for redistribution. In wetter years (positive f(x)), more nitrogen is routed via water; in drier years (negative f(x)), wind becomes the dominant vector.

S2.2 Synthetic rainfall-variability experiments

To generate the modified rainfall scenarios, we used NOAA climate data from two representative climate divisions in the southwestern United States. These divisions were selected to define the dry and wet climate endmembers of the regional aridity gradient.

- Dry climate endmember (Southwest Arizona): Mean Annual Rainfall (MAR) = 132.1 mm; Coefficient of Variation (CoV) = 38.1%
- Wet climate endmember (Northern Plateau New Mexico): MAR = 286.21 mm; CoV = 22.80%

The modified rainfall scenarios were generated by adjusting the CoV, while maintaining the mean rainfall constant for each scenario. Specifically, the new CoV for each scenario was calculated as follows:

$$New\ CoV = (1 - w_{CoV}) \times CoV_1 + w_{CoV} \times CoV_2$$

where CoV_1 and CoV_2 represent the CoV of the dry and wet endmembers respectively. The weights (w_{CoV}) ranged from 0 to 1 to generate different levels of variability between the two extremes. The new standard deviation (new Std) was then derived from the calculated new CoV using the mean rainfall as follows:

$$New\ Std = \frac{New\ CoV}{100} \times mean\ rainfall$$

Once the new standard deviation was determined, the original interpolated rainfall series was adjusted to achieve the desired level of variability while keeping the mean unchanged. Specifically, the adjustment was made by scaling the original series to match the target standard deviation, ensuring that each generated scenario preserved the original mean rainfall but exhibited the intended level of variability (Figure 1d in the main Manuscript).

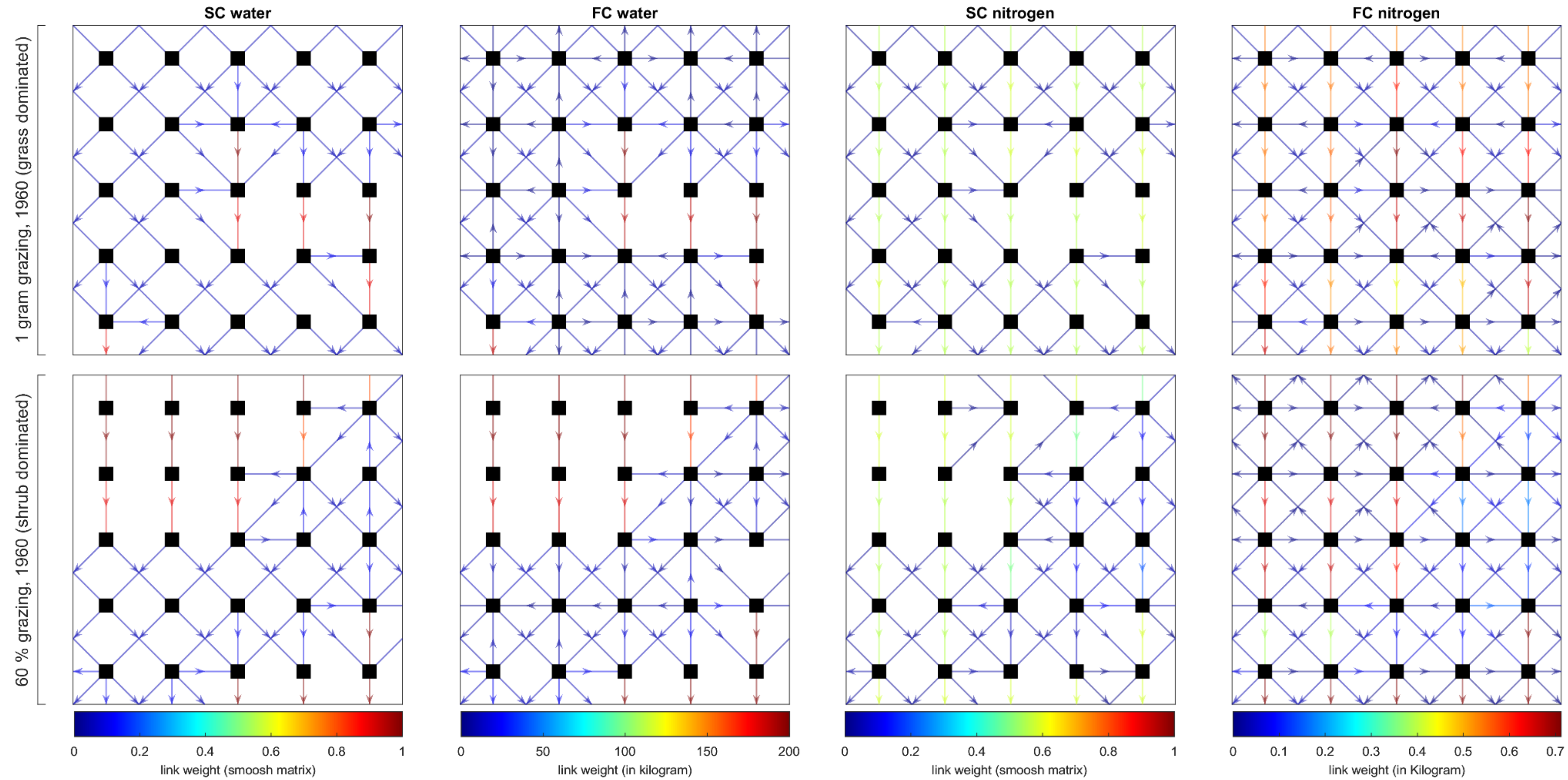

Figure S1. Structural connectivity (SC) and functional connectivity (FC) networks for water and nitrogen in the wet climate endmember under downslope wind conditions. Panels (a–d) show SC and FC networks for water (a–b) and nitrogen (c–d) under low grazing intensity (1 $g/m^2/year$) at the simulation year 1960. Panels (e–h) show corresponding SC and FC networks for water (e–f) and nitrogen (g–h) under high grazing intensity (60% of available grass biomass) at the same time step. SC networks are constructed based on vegetation structure and vector redistribution matrices, while FC networks incorporate modelled flows of water and nitrogen based on resource availability and transport dynamics across the landscape. For visualisation, only the central 5×5 nodes of the full 100×100 node grid (totalling 10,000 nodes) is shown. Because SC and FC networks are constructed based on vector-driven transport (wind, water, and animals), opposing flows between node pairs can cancel out, resulting in cases where a pathway exists in one network but not the other.

S3 Additional Results supporting RQ 1 (Drivers of regime shifts)

The main manuscript (Section 4.1; Figures 1–2) focuses on simulations using two natural climate divisions that represent contrasting mean annual rainfall. These correspond to the dry and wet climate endmembers used throughout this study. In this section, we provide the complete biomass time series and spatial map outputs from the dry endmember, modified dry endmember (with reduced rainfall variability), wet endmember, and modified wet endmember (with increased rainfall variability), to examine how the rainfall coefficient of variation (CoV) influences grass–shrub regime shifts.

Separate grass-only and shrub-only spatial maps (Figures S7 and S8) complement the total biomass outputs(Figure 2) presented in the main text. Across both the natural and modified rainfall scenarios, the large-scale spatial arrangement of grass and shrub cover remains consistent. A comparison between the spatial patterns in the main text (Figure 2) and those shown here (Figure S6) confirms that altering rainfall variability has minimal impact on the overall distribution of vegetation types.

S3.1 Time-series of biomass (Figures S2 & S4)

In the modified dry endmember (low mean annual rainfall and reduced CoV), time series outputs (Figure S3) reveal persistent grass dominance under low grazing (1 g m^{-2} $year^{-1}$), with shrub presence remaining negligible. At moderate grazing (30%), grass fragmentation becomes apparent by the 1920s, followed by scattered shrub emergence around the 1940s. Under high grazing (45–60%), shrub biomass increases sharply, forming a sparse mosaic by the mid-century and nearly complete shrub dominance by 2000 in the 60% grazing case.

In the modified wet endmember (high rainfall and increased CoV), results shown in Figure S5 indicate that grass cover remains extensive under low grazing, with very limited shrub encroachment. With 30% grazing, isolated shrubs emerge around the mid-20th century. When wind is upslope, these shrubs form faint aligned bands, while downslope wind produces more irregular, patchy patterns. Under 45-60% grazing, shrub biomass increases more slowly than in the dry endmember. Even by 2020, significant areas of grass remain under the 45% grazing scenario. This stands in contrast to the modified dry endmember (Figure S3), where shrub dominance is nearly complete under similar grazing pressures.

A direct inspection of the separate grass-only and shrub-only maps (Figure S7 & S8) confirms a near-complete mutual exclusion: wherever shrub biomass exceeds a minimal threshold, grass is essentially absent, and vice versa. This binary representation of grass and shrub biomass justifies the main text's use of a two-colour total-biomass map (Figure 6) to convey spatial change without separate layer plots.

The primary manuscript emphasizes simulations under natural rainfall and downslope wind conditions because changes in rainfall variability (CoV) or wind direction do not substantially alter the spatial extent or outcome of vegetation transitions (Figures 1, 2, S2-S6). These secondary drivers mainly affect the timing of transitions and the geometry of shrub expansion, rather than the presence or location of regime shifts. Therefore, focusing on natural-rainfall and downslope-wind scenarios allows the analysis to focus on the dominant controls: mean annual rainfall and grazing intensity.

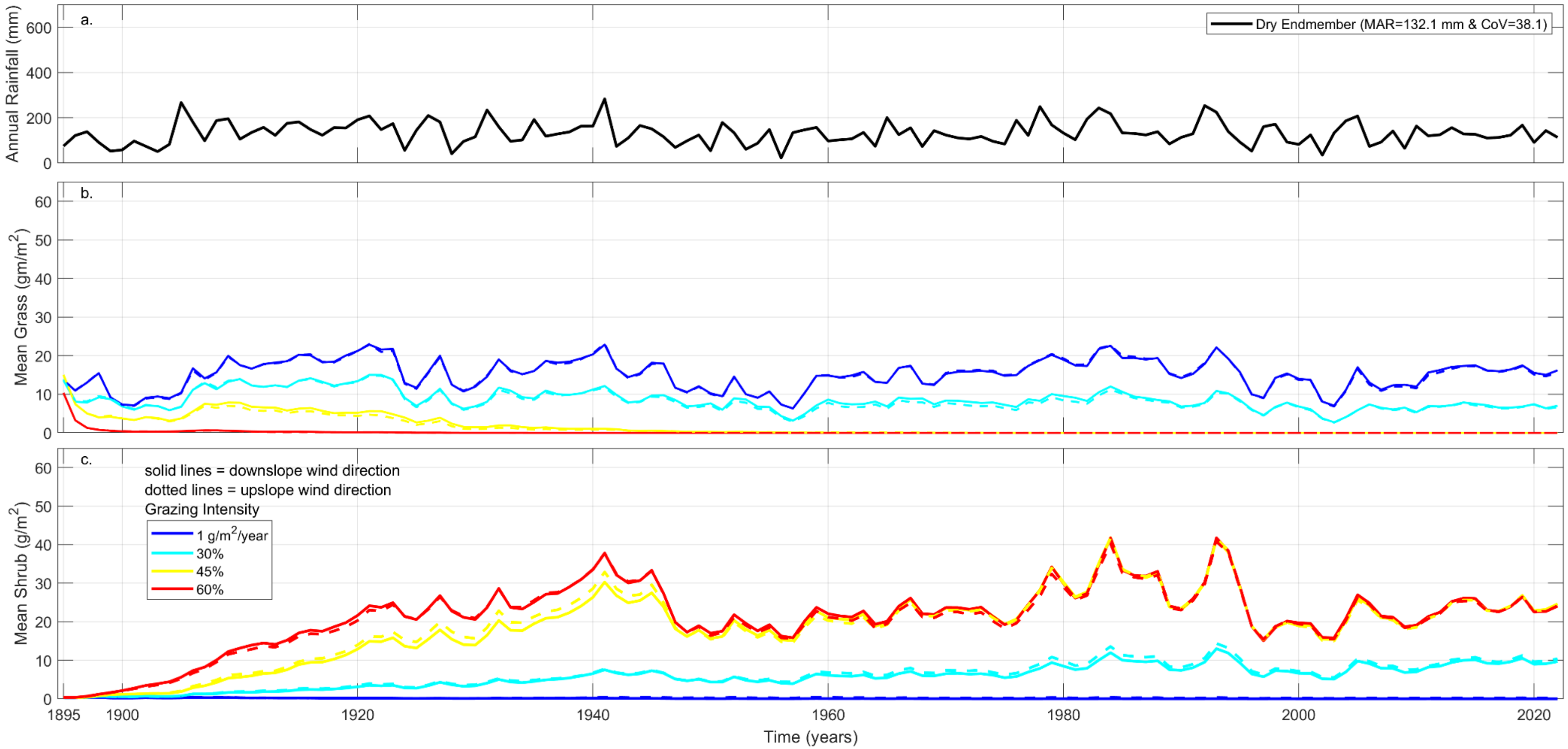

Figure S2. Time series of simulated annual mean grass and shrub biomass (g/m²) for the dry climate endmember under four grazing intensities (1 g/m²/year, 30%, 45%, and 60% of available grass biomass) and two wind directions (upslope and downslope). Results correspond to simulations using historical rainfall variability. Outcomes for the modified dry endmember rainfall variability scenario are provided in Figure S3.

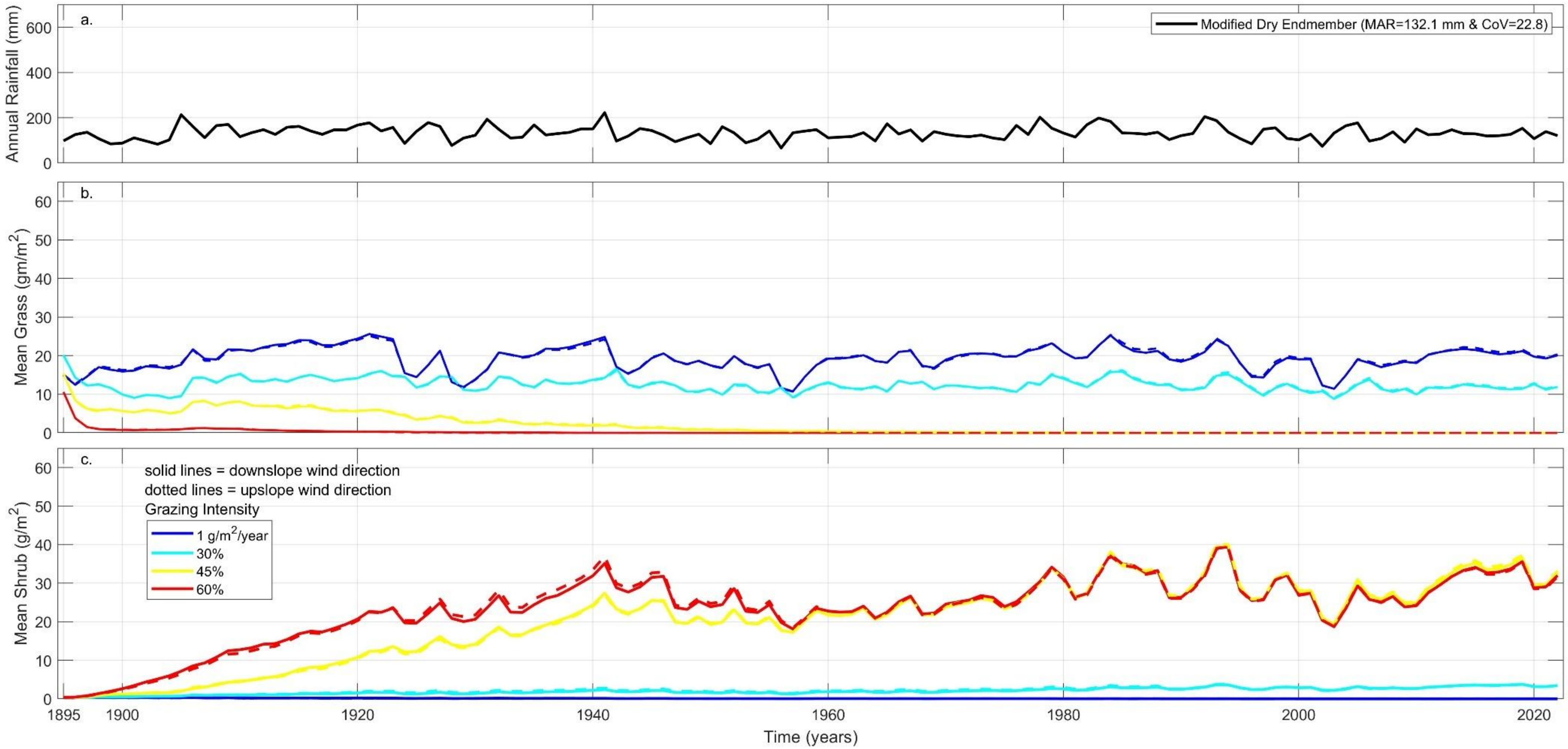

Figure S3. Time series of mean grass and shrub biomass (g/m²) under varying grazing intensities and wind directions for the modified dry endmember. These scenarios apply reduced rainfall variability (lower CoV) while maintaining the original mean annual rainfall.

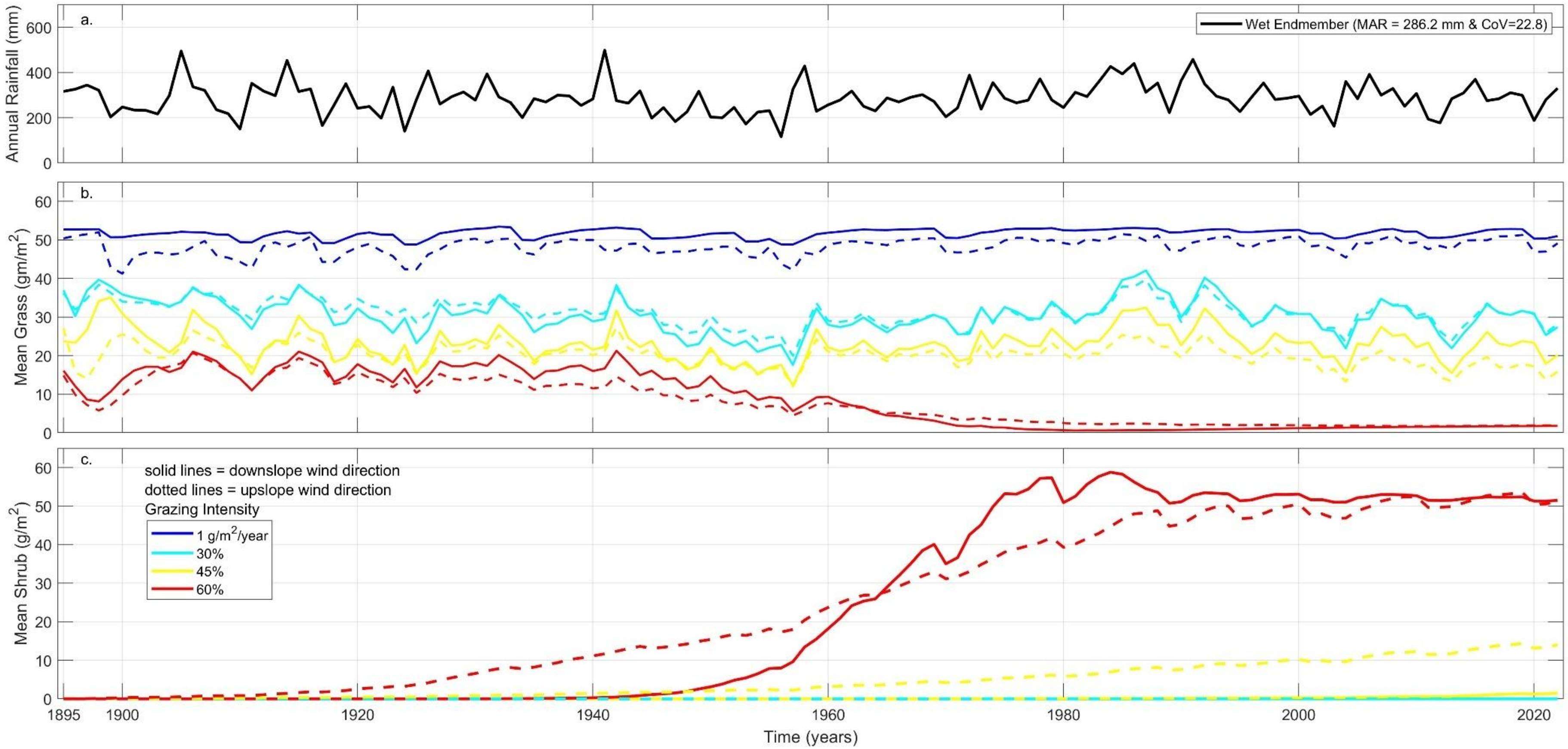

Figure S4. Time series of simulated annual mean grass and shrub biomass (g/m²) for the wet climate endmember under four grazing intensities (1 g/m²/year, 30%, 45%, and 60% of available grass biomass) and two wind directions (upslope and downslope). Results correspond to simulations using historical rainfall variability. Outcomes for the modified wet endmember rainfall variability scenario are provided in Figure S5.

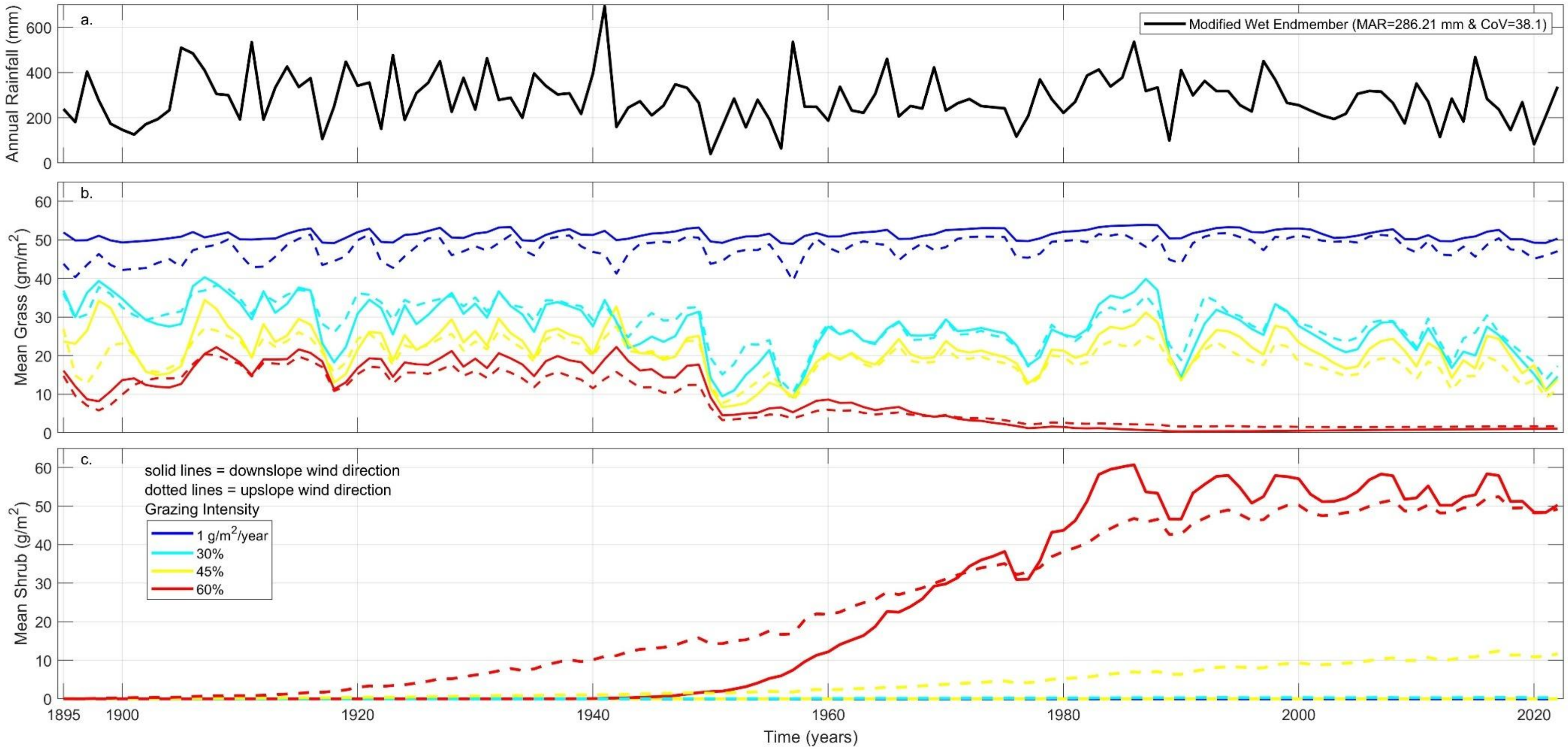

Figure S5. Time series of mean grass and shrub biomass (g/m²) under varying grazing intensities and wind directions for the modified wet endmember. These scenarios apply increased rainfall variability (higher CoV) while preserving the original mean annual rainfall.

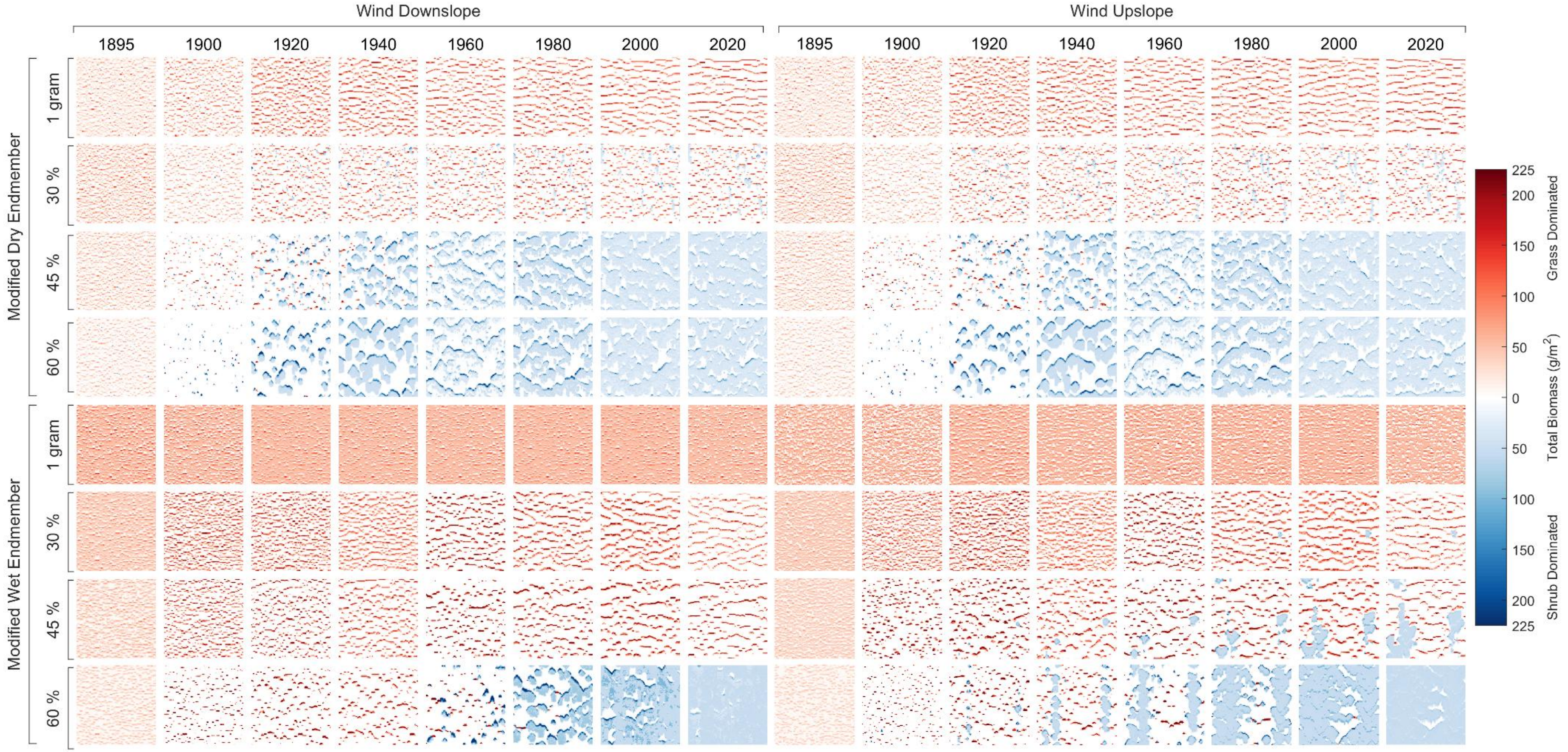

Figure S6. Spatial distribution of total biomass (g/m^2), showing grass- and shrub-dominant vegetation types at selected time steps (1895, 1900, 1920, 1940, 1960, 1980, 2000, and 2020) for the modified dry and modified wet endmembers. Results are shown for upslope and downslope wind directions and four grazing intensities: 1 g/m^2/year, 30%, 45%, and 60%.

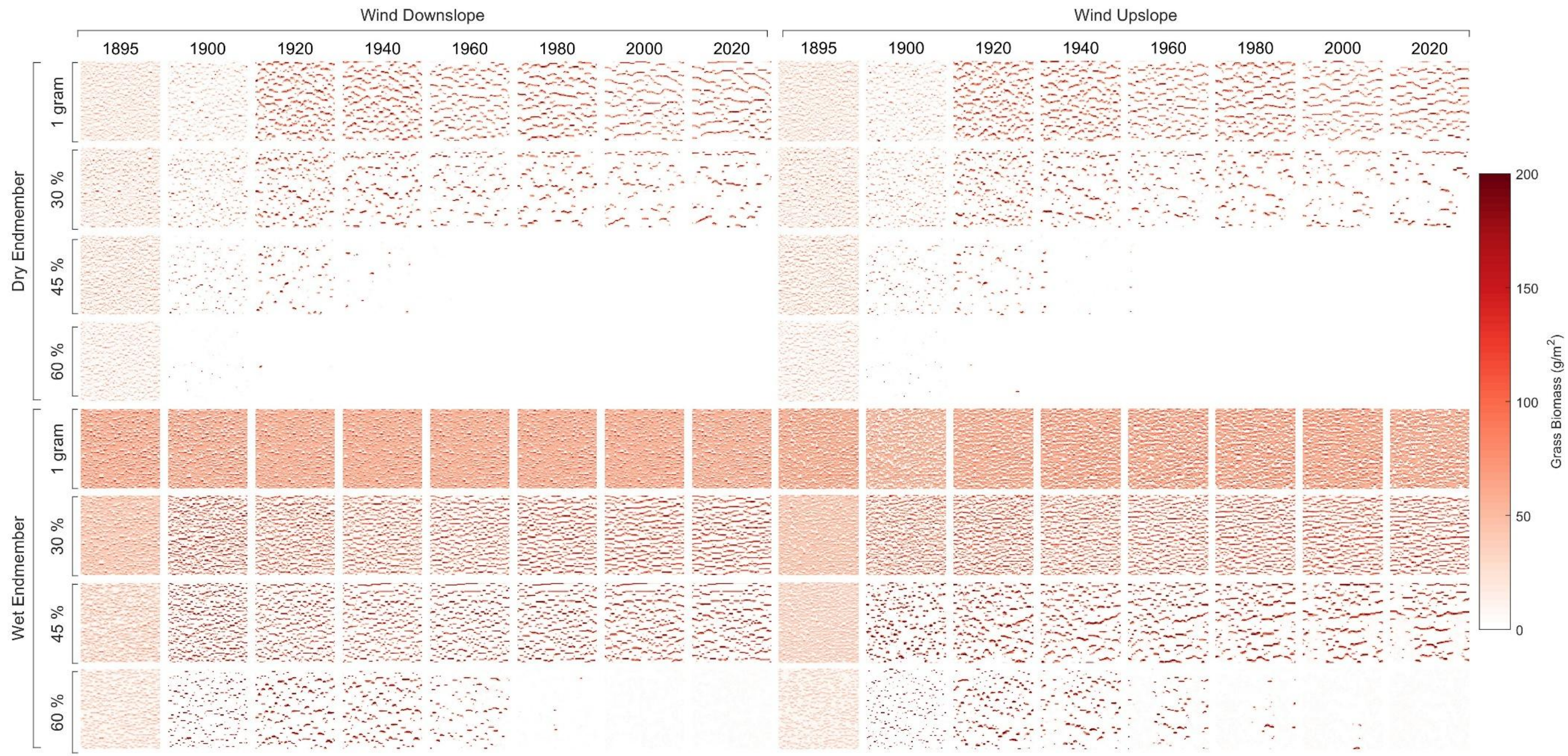

Figure S7. Spatial distribution of grass biomass (g/m²/year) at specific time steps (1895, 1900, 1920, 1940, 1960, 1980, 2000, and 2020) for the dry and wet endmembers. Results are shown for upslope and downslope wind directions across four grazing intensities: 1 g/m²/year, 30%, 45%, and 60%.

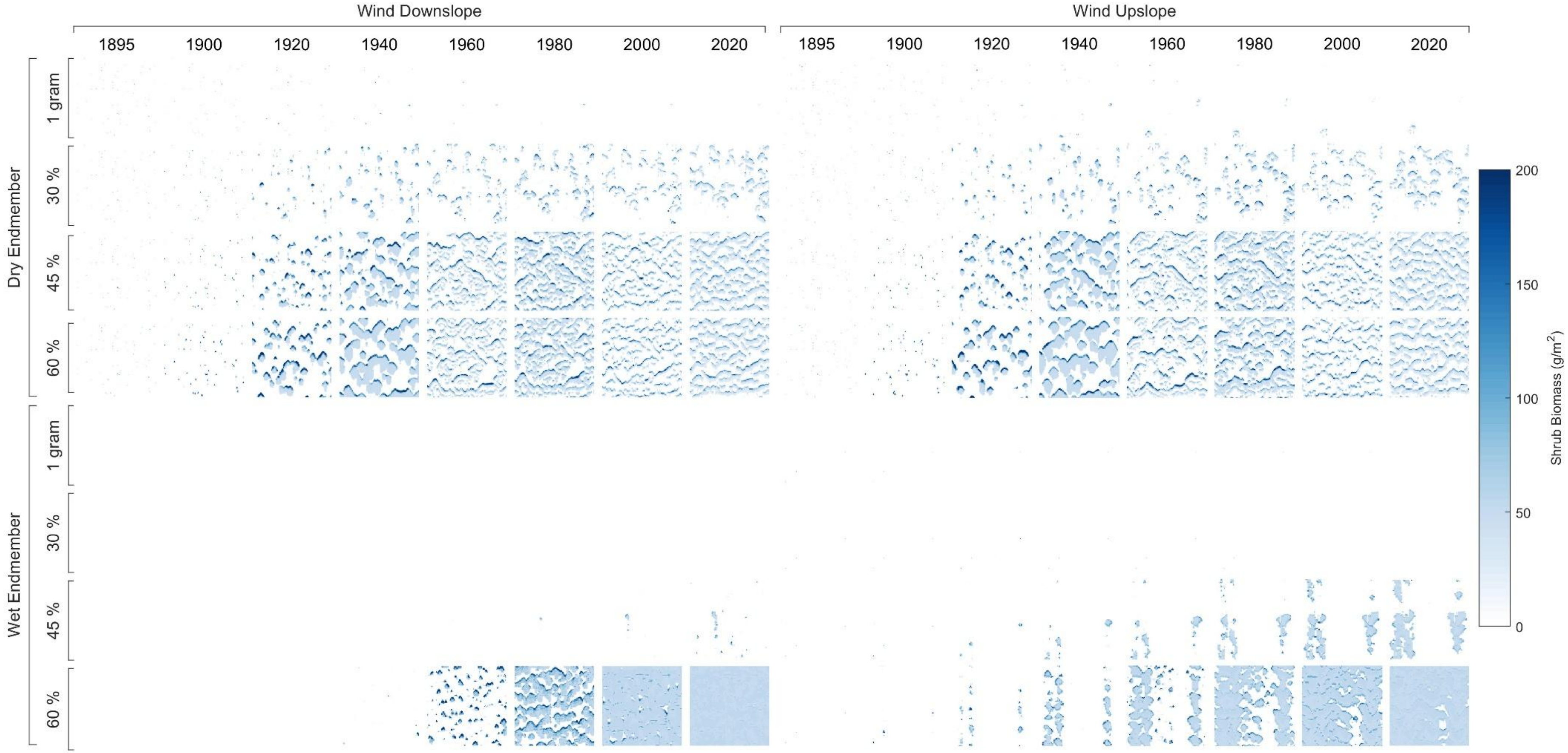

Figure S8. Spatial distribution of shrub biomass (g/m²) at specific time steps (1895, 1900, 1920, 1940, 1960, 1980, 2000, and 2020) for the dry and wet endmembers. Results are shown for upslope and downslope wind directions across four grazing intensities: 1 g/m²/year, 30%, 45%, and 60%.

S4 Additional results supporting RQ 2 (Early-warning indicators)

S4.1 Global Efficiency (GE) Trends

S4.1.1 Structural Connectivity of Water (SC water):

In both the dry and wet climate endmembers, GE of SC water displays a consistent decline with increasing grazing intensity. This shows a shift in water redistribution from a multi-directional network to largely unidirectional downslope flow due to the absence of vegetative sinks. In the dry endmember (Figure S9 c), GE remains relatively high under low grazing (1 g/m² and 30%) and shows a steady increase from ~1910 onwards. Notably, in the 60% scenario, GE of SC water continues to increase with two major dips in 1950s and 1990s, coinciding with the establishment and expansion of shrub cover (Figure S9 b and c). This rebound suggests that shrubs reorganize the spatial connectivity of the landscape, forming new structural pathways for water redistribution.

In the wet endmember (Figure S10 c), SC water GE starts at higher values due to the denser and more continuous vegetation cover. Under all grazing scenarios except 60 %, the GE remains constant throughout. With 60% grazing, SC water GE gradually increase from the 1970s and again becomes constant around 1990s (Figure S10 b).

S4.1.2 Functional Connectivity of Water (FC water):

The GE of FC water exhibits pronounced temporal variability, closely tracking interannual fluctuations in rainfall (Figure S9 d and 10 d). In both dry and wet endmember, peaks in annual precipitation consistently align with spikes in FC water GE, highlighting the dominant influence of hydrologic inputs on realized water flow pathways. Under 60% grazing intensity, the magnitude of these fluctuations is notably dampened during the early stages of the simulation when grasses still dominate the landscape. However, as shrubs begin to establish and eventually become dominant, the GE of FC water increases markedly. This shift is especially pronounced in the dry endmember, where a sharp rise in GE is observed from the 1960s through the 1990s, reaching a peak during the early 1990s. Following this peak, FC water GE gradually declines toward the end of the simulation. In contrast, the wet endmember exhibits a more gradual increase and less pronounced peak, reflecting a more buffered response to vegetation change and grazing intensity.

S4.1.3 Structural Connectivity of Nitrogen (SC nitrogen):

Trends in SC nitrogen GE follow similar patterns to SC water but with sharper changes under high grazing. In the dry endmember (Figure S9), under 60% grazing, SC nitrogen GE increases dramatically between 1925 and 1950, aligning with the onset and expansion of shrub dominance. This suggests that structural nitrogen connectivity becomes more efficient as shrubs reorganize the patch network. Under lower grazing levels, the metric remains stable or slightly declining.

The wet endmember (Figure S10) shows delayed but pronounced increases in SC nitrogen GE under high grazing, beginning in the late 1950s. Under 45% and 60% grazing, the GE increases after a brief initial decline, indicating that shrubs in wetter environments establish a structurally connected system for nitrogen redistribution.

S4.1.4 Functional Connectivity of Nitrogen (FC nitrogen):

The GE of FC nitrogen is consistently the lowest among all metrics and is highly variable, reflecting the episodic and constrained movement of nitrogen through structural pathways. In the dry endmember, under minimal grazing, the GE of FC nitrogen remains near zero (Figure S9). At 45% and 60% grazing, it begins to increase only after 1930–1940, in step with shrub expansion, though values remain modest overall. In the wet endmember, the rise is more evident: under 60% grazing, FC nitrogen GE increases gradually from 1950 onwards, peaking around 1980, again tracking with shrub establishment (Figure 10). This suggests that nitrogen redistribution becomes increasingly organized as shrublands replace grass-dominated patches.

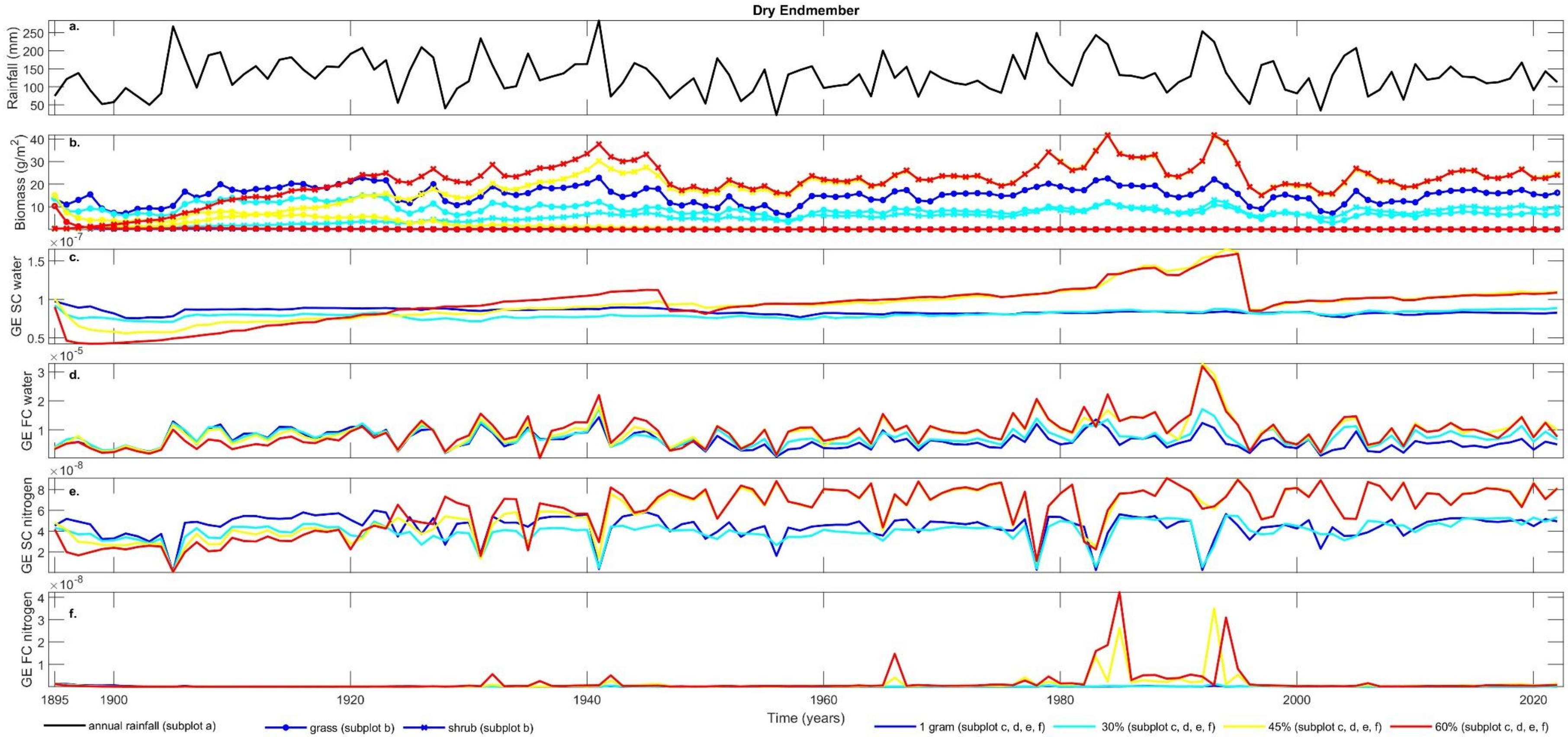

Figure S9. Time series depicting the annual rainfall (mm), mean grass biomass (g/m²), mean shrub biomass (g/m²), and global efficiency of SC water, FC water, SC nitrogen and FC nitrogen networks for the dry endmember. Data is presented for downslope wind direction and across four grazing intensities: 1 gram, 30%, 45%, and 60%.

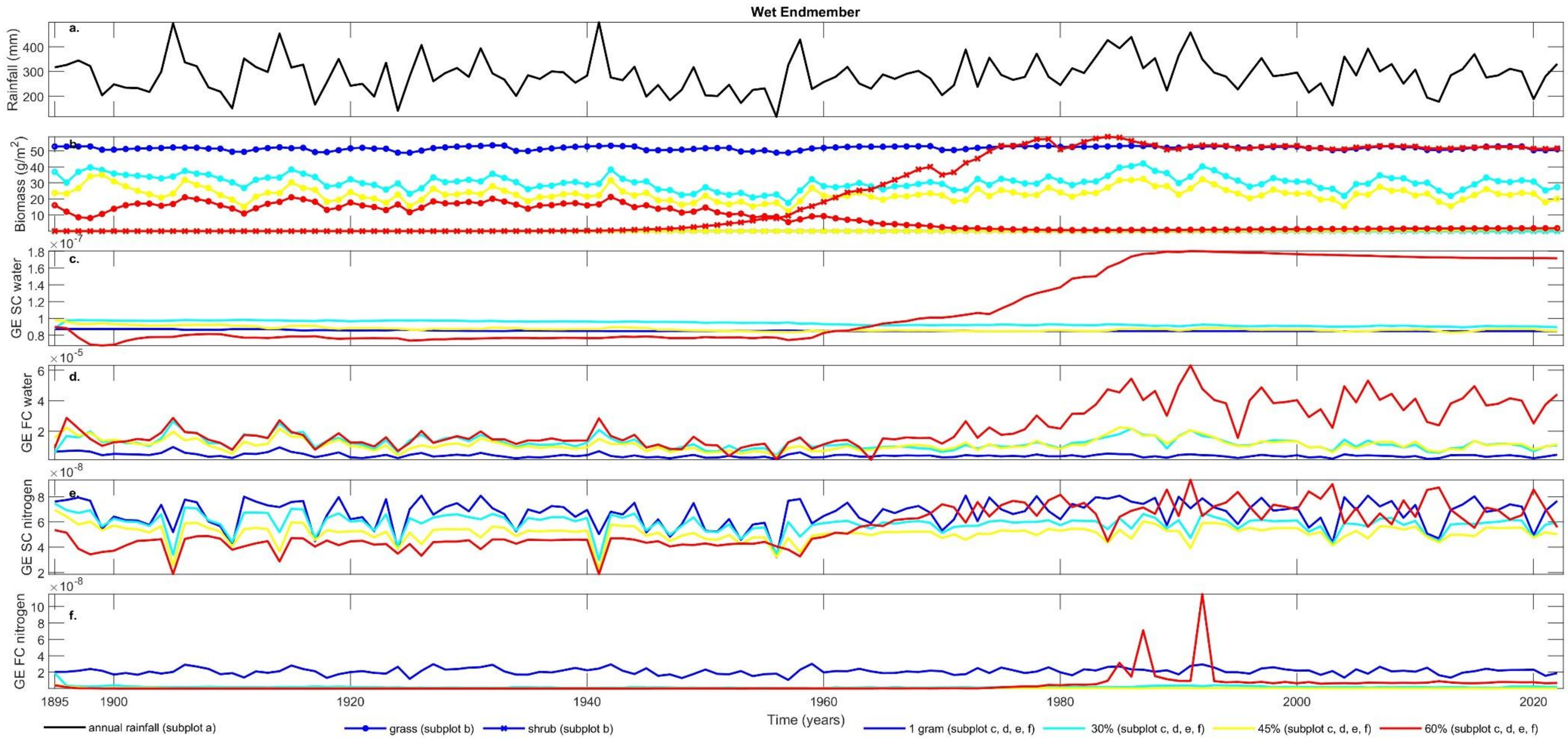

Figure S10. Time series depicting the annual rainfall (mm), mean grass biomass (g/m²), mean shrub biomass (g/m²), and global efficiency of SC water, FC water, SC nitrogen and FC nitrogen networks for the wet endmember. Data is presented for downslope wind direction and across four grazing intensities: 1 gram, 30%, 45%, and 60%.

S4.2 Centralization Degree (CD) Trends

4.2.1 CD of SC water:

The Centralization Degree (CD) of structural connectivity networks captures the extent to which connectivity is concentrated through a small number of dominant patches. In the dry endmember (Figure S11), the CD of SC water remains consistently low and stable under minimal and moderate grazing intensities (1 g/m² and 30%), indicating a relatively decentralized and evenly distributed network structure. However, under higher grazing intensities (45% and 60%), CD of SC water exhibits a progressive increase from approximately 1910 to 1990, signalling a growing dependence on a limited number of key patches for water redistribution as the landscape becomes increasingly fragmented. Notable declines in CD are observed around 1945 and 1990, potentially corresponding to vegetation shifts and temporary changes in connectivity patterns. After 1990, CD stabilizes, likely due to the widespread establishment of shrubs, which reduces network centralization by enabling more distributed connectivity.

In the wet endmember (Figure S12), a similar but temporally delayed pattern emerges. Under 60% grazing, the CD of SC water remains relatively low and stable until around 1970, after which it increases sharply, peaking in the mid-1980s coinciding with the onset and progression of shrub encroachment. Following this transition, CD plateaus, reflecting the establishment of a more spatially distributed shrub-dominated connectivity structure. This shift suggests a move from a fragmented, centralized network to a more uniform and resilient configuration as shrubs become dominant.

Furthermore, the temporal patterns of CD in SC water differ significantly from those observed in FC water, SC nitrogen, and FC nitrogen, all of which exhibit higher sensitivity to interannual rainfall variability and show more fluctuation-driven behaviour.

4.2.2.2 CD of FC water:

In the dry endmember (Figure S11), CD values for FC water remain relatively low but variable under low grazing intensities (1 g/m² and 30%). As grazing pressure increases, especially under 45% and 60% grazing, CD values gradually rise over time. The most prominent increase is observed under the 60% grazing scenario, where CD begins increasing around the 1940s and peaks in the early 1990s. This trend suggests a growing reliance on fewer, more central patches for water redistribution as the system transitions from grass to shrub dominance. After the 1990s, CD values decline slightly or stabilize, possibly due to a more widespread distribution of shrubs leading to a more evenly connected system.

In the wet endmember (Figure S12), the pattern differs. Under low grazing intensity (1 g/m²), CD values are consistently higher and show strong year-to-year variability. This suggests that under relatively intact vegetation cover, water flows are more centralized, possibly concentrated through persistent grass patches. In contrast, under moderate grazing (30% and 45%), CD values are lower and more stable, indicating a more distributed flow pattern. Under 60% grazing, CD remains low initially but increases sharply around 1970, aligning with the period when shrubs begin to dominate. This rise is short-lived, and CD declines again after 1985, stabilizing at lower levels toward the end of the simulation.

Overall, these trends show that functional hydrological connectivity becomes more centralized under high grazing in drier climate, while wetter arid climate display more dynamic shifts linked to vegetation transitions.

S4.2.3 CD of SC nitrogen

In both dry and wet endmembers, the centralization degree (CD) of structural nitrogen connectivity exhibits distinct temporal patterns shaped by grazing intensity and rainfall variability (Figure S11 and S12).

In the dry endmember, CD of SC nitrogen starts at similarly low levels across all grazing intensities, indicating initially well-distributed nitrogen redistribution networks. As the simulation progresses, divergence emerges. Under low grazing (1 g/m^2 and 30%), CD values display strong interannual variability, fluctuating closely in response to rainfall events (Figure S8). By contrast, under higher grazing intensities (45% and 60%), CD values become progressively more stable, particularly from ~1930 onwards. The 60% grazing scenario shows the most consistent CD trend, remaining relatively flat (Figure S11).

In the wet endmember, CD of SC nitrogen is more variable early in the simulation, with initial differences between grazing treatments (Figure S12). At the beginning, 60% grazing produces the highest CD values, while 1 g/m^2 grazing yields the lowest. However, a gradual convergence occurs after 1980. Notably, CD under the 60% grazing scenario declines steadily after peaking around 1980, showing sensitivity to vegetation transitions and possibly indicating a shift to a more spatially balanced nitrogen connectivity structure. By 2020, CD values for both low and high grazing treatments are nearly identical, suggesting a convergence in network centralization regardless of initial grazing pressure (Figure S12).

S4.2.4 CD of SC nitrogen

The CD of FC nitrogen follows patterns that are closely aligned with its structural counterpart. In the dry endmember, CD values under low grazing (1 g/m^2 and 30%) show higher interannual variability, again closely tracking rainfall fluctuations (Figure S11). As grazing intensity increases, this variability diminishes. The 60% grazing scenario maintains a relatively steady CD after 1940, with few fluctuations, indicating that nitrogen flow becomes funnelled through a small number of dominant nodes. These trends suggest that under intensive grazing, nitrogen transport becomes increasingly reliant on fewer, spatially concentrated patches (Figure S11).

In the wet endmember, CD of FC nitrogen mirrors the temporal evolution observed in SC nitrogen. Initially, CD is highest for 60% grazing and lowest for 1 g/m^2, suggesting early dominance of centralized nitrogen flow under heavy grazing (Figure S12). However, starting around 1980, CD for the 60% grazing scenario begins to decline, showing more pronounced sensitivity to interannual rainfall variability. By the end of the simulation (~2020), CD values for all grazing treatments converge, similar to the SC nitrogen case (Figure S9). The decline in CD under high grazing after 1980 likely corresponds to the broad spatial establishment of shrubs, redistributing nitrogen more uniformly and reducing network centralization.

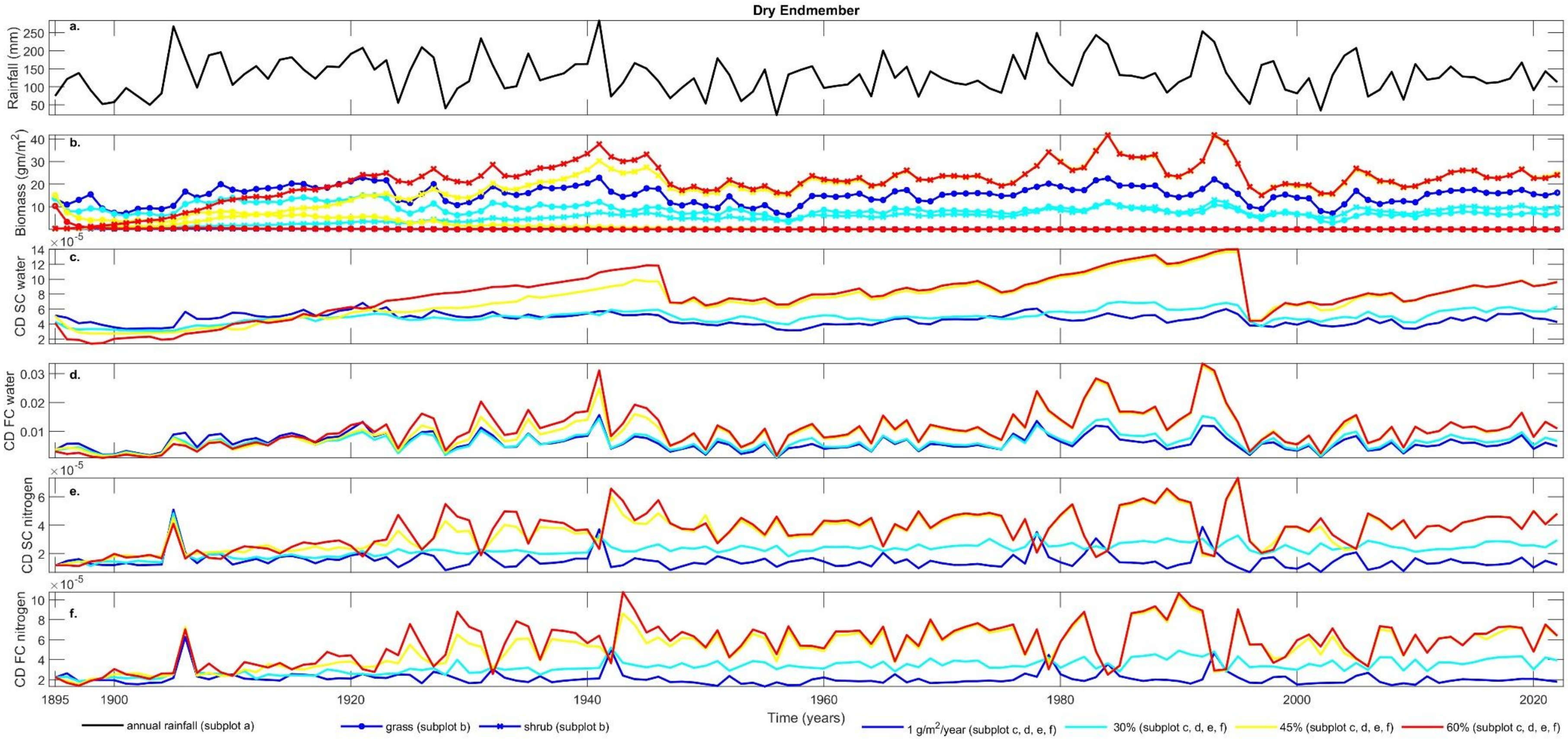

Figure S11. Time series depicting the annual rainfall (mm), mean grass biomass (g/m²), mean shrub biomass (g/m²), and centralisation degree (CD) of SC water, FC water, SC nitrogen and FC nitrogen networks for the dry endmember. Data is presented for downslope wind direction and across four grazing intensities: 1 gram, 30%, 45%, and 60%.

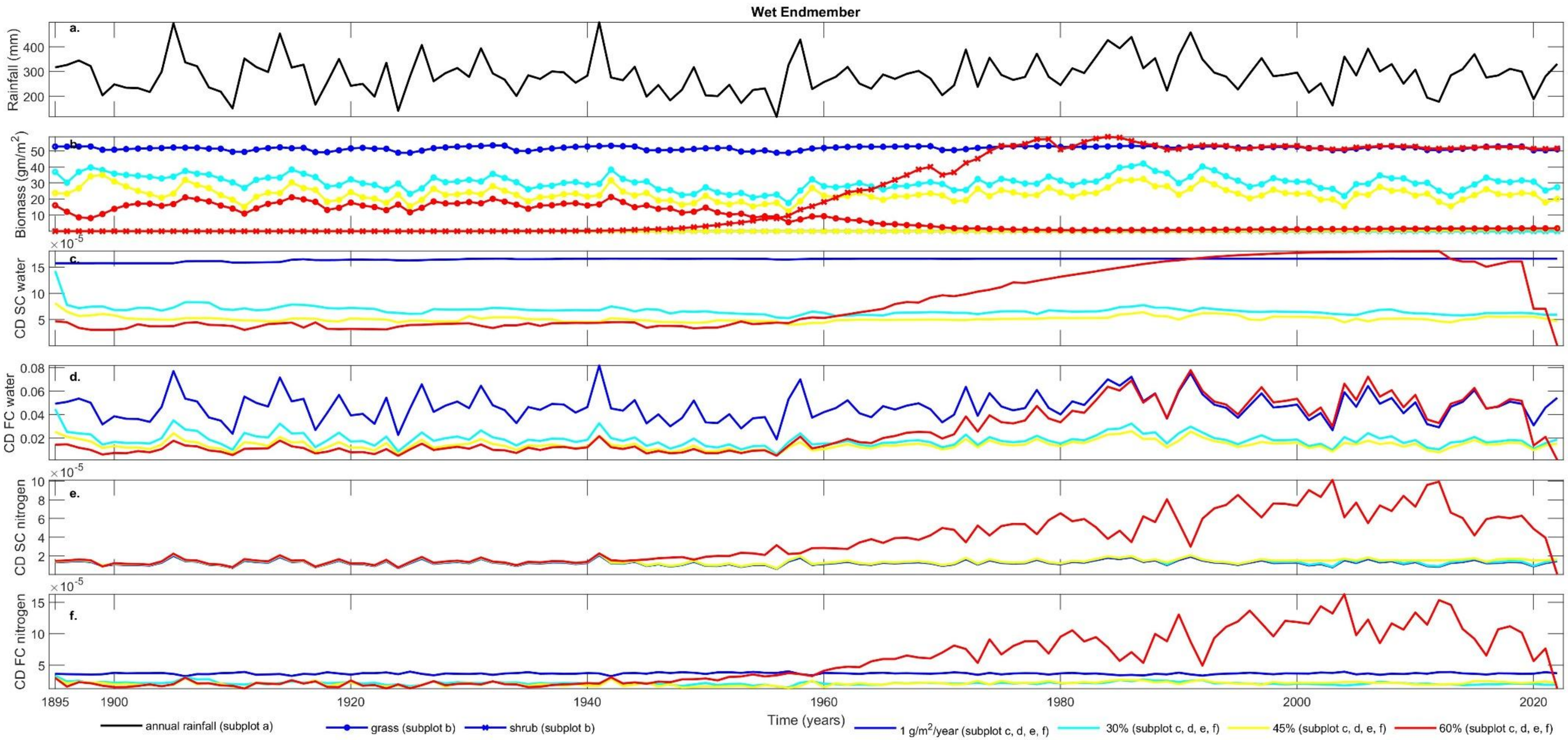

Figure S12. Time series depicting the annual rainfall (mm), mean grass biomass (g/m²), mean shrub biomass (g/m²), and centralisation degree (CD) of SC water, FC water, SC nitrogen and FC nitrogen networks for the wet endmember. Data is presented for downslope wind direction and across four grazing intensities: 1 gram, 30%, 45%, and 60%.

S4.3 Betweenness Centrality (BC) Trends

S4.3.1 BC of SC Water and FC Water

Betweenness centrality (BC) in the structural (SC) and functional (FC) water networks indicates how crucial individual patches are for mediating water flow across the landscape. For both dry and wet endmember, the temporal trends of mean BC values for SC and FC water are closely aligned, with only minor deviations (Figures S13 and S14). This similarity suggests that functional water redistribution is largely constrained by the underlying structural connectivity, and FC water BC is not strongly influenced by interannual rainfall variability.

In the dry endmember (Figure S13), BC under low grazing intensities (1 g/m^2 and 30%) remains low and stable throughout the simulation, reflecting a decentralized network where water redistribution is evenly shared across many patches. Under higher grazing intensities (45% and 60%), BC increases sharply from ~1920, peaking around 1940–1945. This early rise corresponds with the onset of grass patch fragmentation. A second, more prominent peak occurs between 1985 and 1995, coinciding with the period of maximum shrub cover. After this point, BC declines, suggesting a return to a more evenly distributed structural network as shrubs dominate the landscape and new flow paths emerge.

In the wet endmember (Figure S14), BC values under 1 g/m^2 grazing start relatively higher than those under higher grazing treatments. However, under the 60% grazing scenario, BC begins to rise gradually around 1970 and peaks in the mid-1980s before stabilizing. This reflects the slower and more gradual vegetation transition in wetter environments, where the landscape retains its structural integrity for longer before entering a shrub-dominated regime.

Spatial maps (Figure S15) reveal that under low grazing, high-BC patches are broadly distributed across the landscape in both regions, indicative of decentralized water flow networks. As grazing pressure increases, these patterns shift towards more distinct areas of high BC, corresponding to key flow routes through increasingly fragmented vegetation. Although the mean BC values for SC and FC water are similar, their spatial distributions diverge notably. In many cases, patches critical to structural connectivity (SC water) do not perfectly overlap with those that dominate functional water flow (FC water), particularly as shrubs expand.

For the dry endmember, SC water BC values start uniformly distributed in early years (e.g., 1895-1920), reflecting the dominance of grass and lack of major structural bottlenecks. As the system transitions, particularly by 1960 and beyond, these values become increasingly heterogeneous, indicating emergent structural bottlenecks.

In the wet endmember, SC water BC under 1 g/m^2 grazing also begins with moderate spatial variation, but under 30% and 45% grazing it becomes more homogeneous. However, under 60% grazing, particularly in later years (1980, 2000, 2020), BC values for SC water become unusually patchy and abrupt. This spatial configuration appears inconsistent and may be a modelling artifact. In contrast, FC water BC values remain spatially logical, with clear contrasts along flow paths that match areas of shrub expansion and topographic redistribution.

S4.3.2 BC of SC Nitrogen and FC Nitrogen

For both SC nitrogen and FC nitrogen networks, mean BC values are generally low, punctuated by a few sharp peaks over time (Figures S16). In the dry endmember, these peaks are more frequent, occurring first around 1945 and then more prominently between 1980 and 2000. These spikes tend to precede or coincide with the peak in mean shrub biomass, suggesting a temporary reorganization of nitrogen redistribution pathways during vegetation transitions. In the wet endmember, the pattern is more subdued, with approximately three notable peaks occurring primarily between 1980 and 2000, reflecting a delayed and more gradual shrub encroachment under wetter conditions.

The spatial distribution of BC also differs markedly between SC nitrogen and FC nitrogen networks (Figure S16). SC nitrogen BC tends to be more uniformly distributed across the landscape, indicating that no single node dominates the structural nitrogen flow. In contrast, FC nitrogen BC maps display more heterogeneous patterns, with certain patches emerging as critical flow intermediaries. This divergence suggests that while the structural potential for nitrogen redistribution remains broadly distributed, actual functional transport becomes increasingly channelled through specific patches as the vegetation regime shifts.

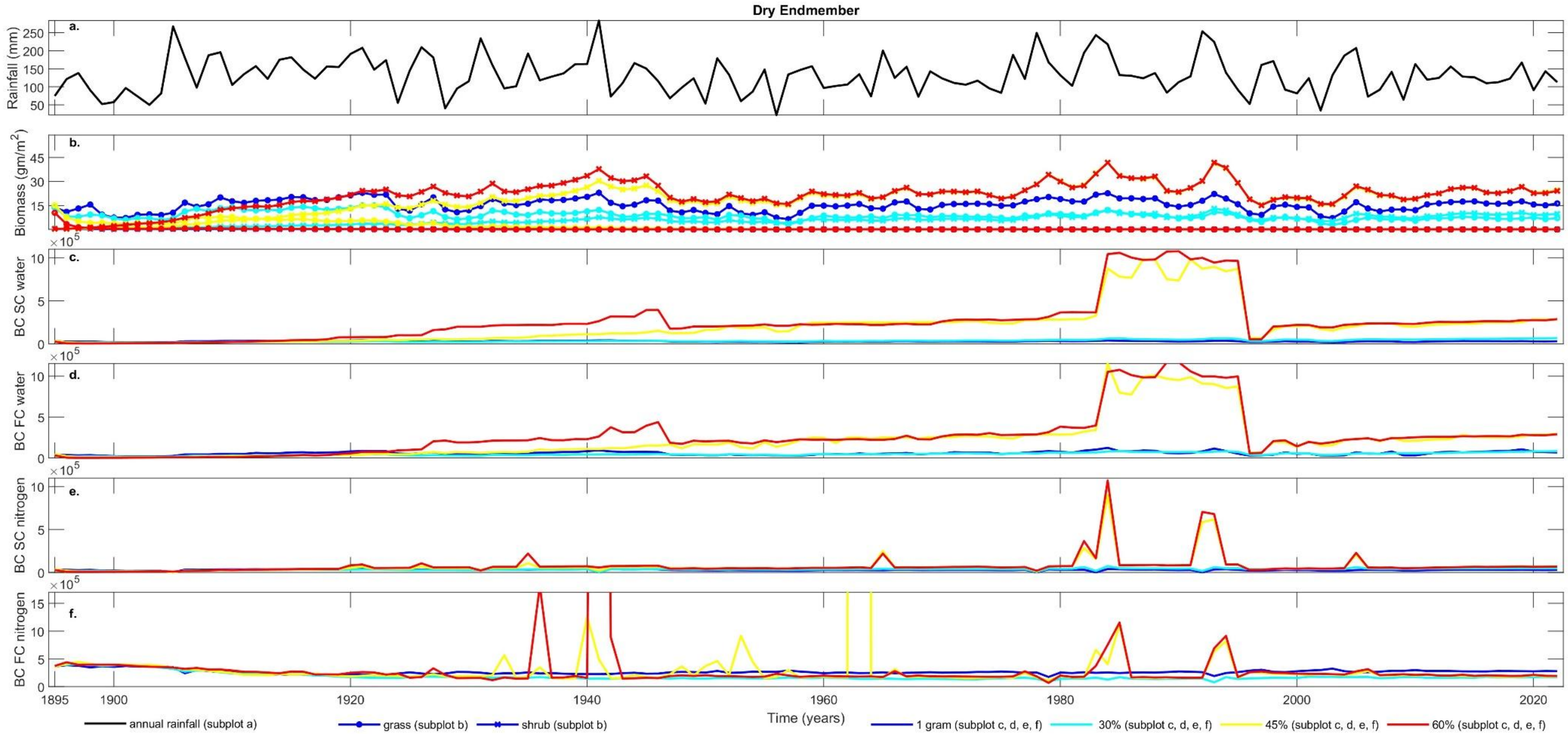

Figure S13. Time series depicting the annual rainfall (mm), mean grass biomass (g/m²), mean shrub biomass (g/m²), and betweenness centrality of SC water, FC water, SC nitrogen and FC nitrogen networks for the dry endmember. Data is presented for downslope wind direction and across four grazing intensities: 1 gram, 30%, 45%, and 60%.

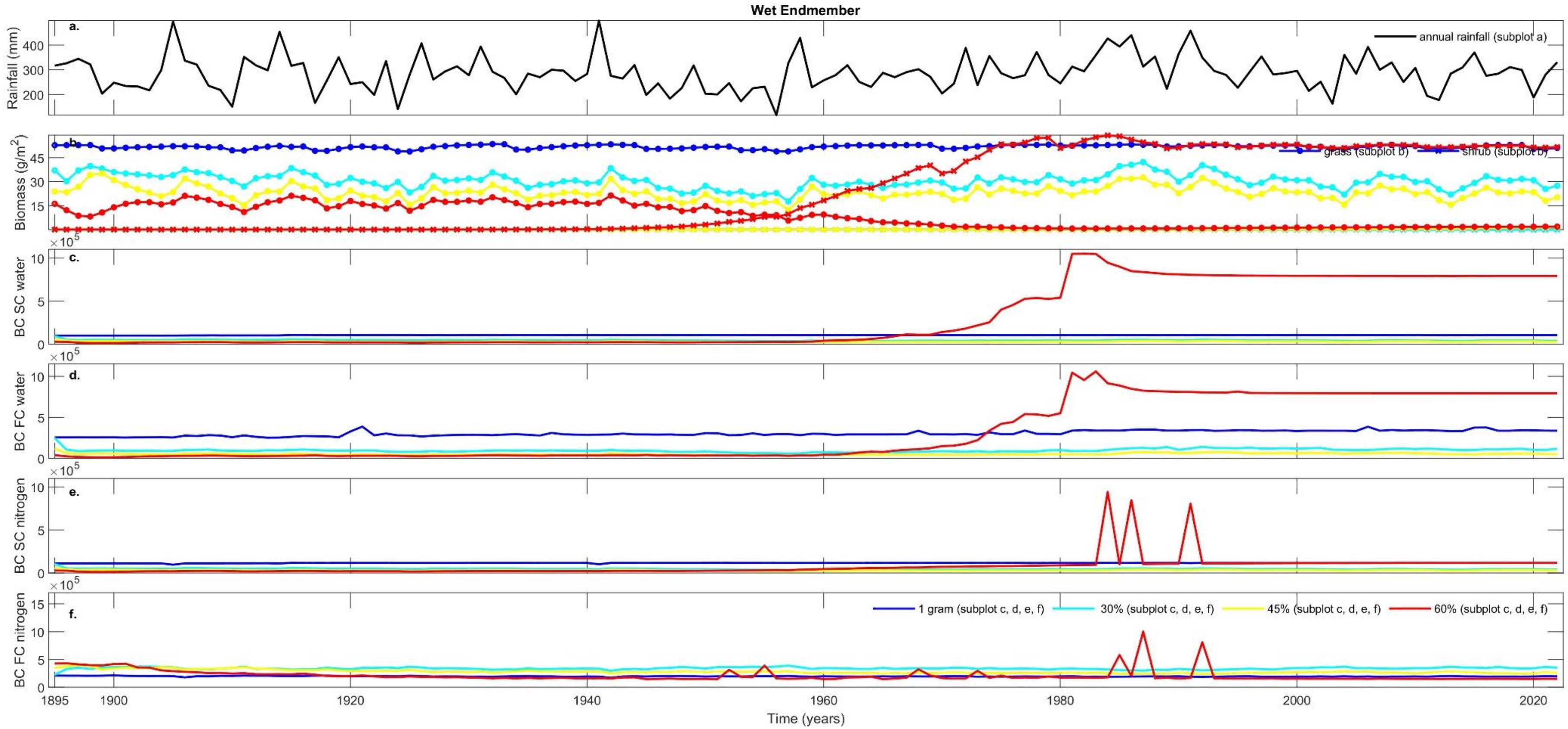

Figure S14. Time series depicting the annual rainfall (mm), mean grass biomass (g/m²), mean shrub biomass (g/m²), and betweenness centrality of SC water, FC water, SC nitrogen and FC nitrogen networks for the wet endmember. Data is presented for downslope wind direction and across four grazing intensities: 1 gram, 30%, 45%, and 60%.

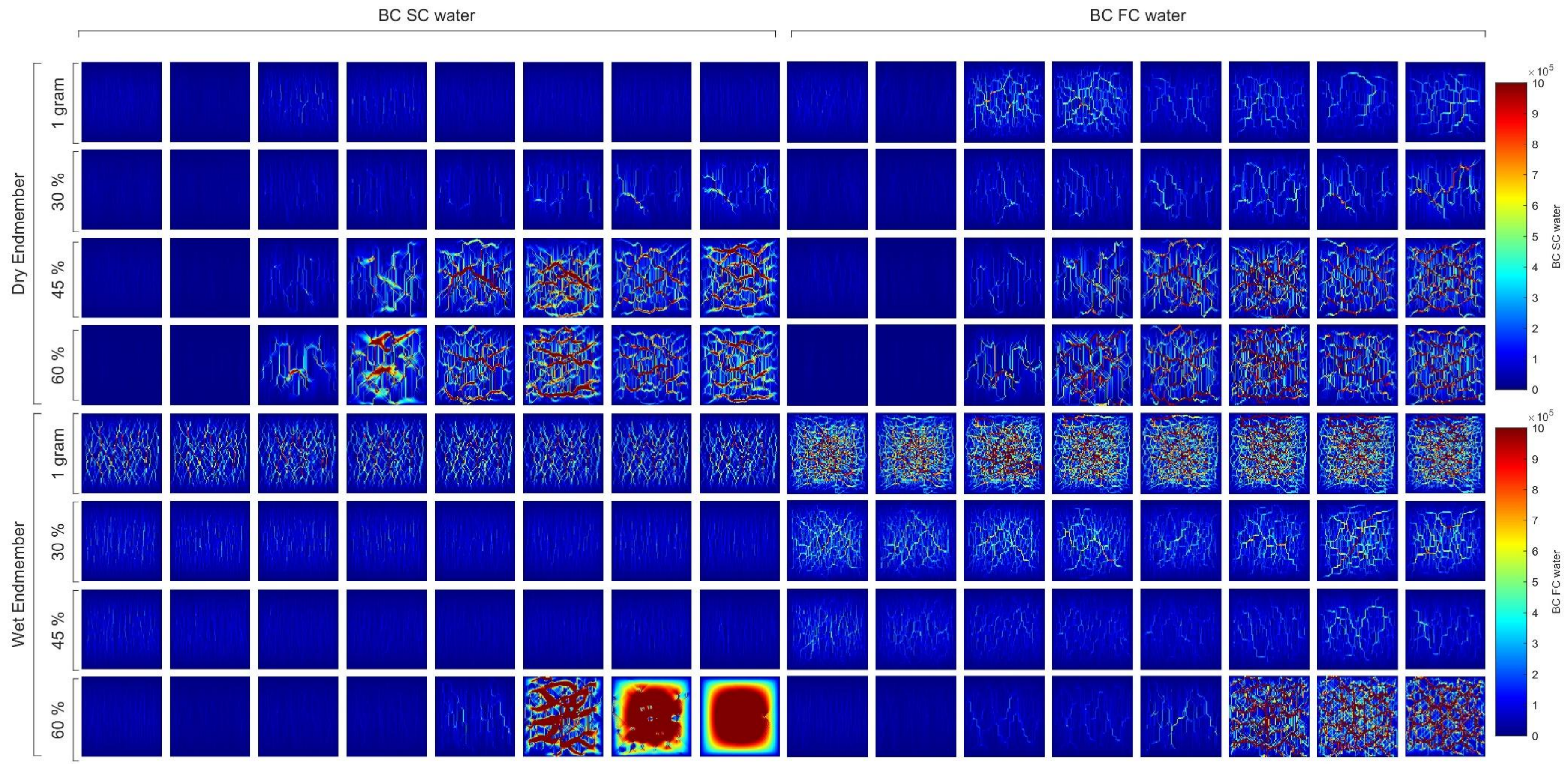

Figure S15. Spatial distribution of Betweenness Centrality (BC) for SC water and FC water network at specific time steps (1895, 1900, 1920, 1940, 1960, 1980, 2000, and 2020) for the dry and wet endmember. Results are presented for downslope wind directions across four grazing intensities: 1 g/m², 30%, 45%, and 60%.

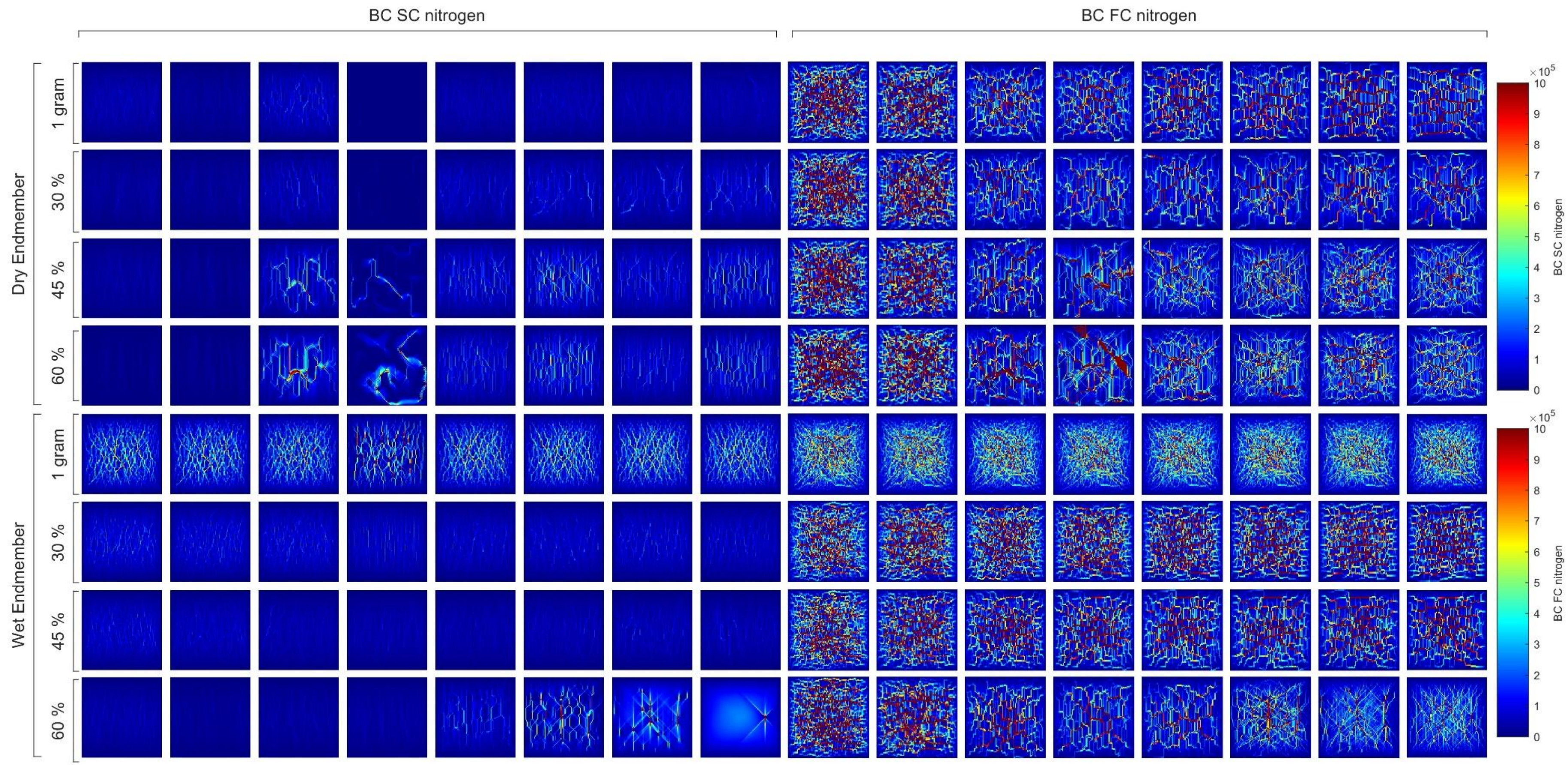

Figure S16. Spatial distribution of Betweenness Centrality (BC) for SC nitrogen and FC nitrogen network at specific time steps (1895, 1900, 1920, 1940, 1960, 1980, 2000, and 2020) for the dry and wet endmember. Results are presented for downslope wind directions across four grazing intensities: 1 g/m², 30%, 45%, and 60%.

S4.4 Weighted Length of Connected Pathways (WLOCOP) Trends

S4.4.1 WLOCOP of SC Water and FC Water

The Weighted Length of Connected Pathways (WLOCOP) for water indicates the average distance water must travel before encountering a vegetated sink. Higher WL values reflect sparser or fragmented vegetation, forcing water to travel longer distances, while lower values suggest a more evenly distributed vegetative cover that facilitates local interception.

In the dry endmember (Figure S17), the mean WLOCOP of SC water shows a strong response to grazing intensity. Under low grazing (1 g/m² and 30%), WLOCOP values remain consistently short throughout the simulation, indicating dense, well-connected grass cover. In contrast, under higher grazing levels (45% and 60%), WLOCOP increases significantly from the early 1920s, peaking around the 1980s, as grass patches fragment and fewer vegetated sinks remain. A sharp decline in WLOCOP follows in the 1990s, coinciding with shrub expansion, which appears to restore vegetative sinks and reorganize the flow network. By the end of the simulation, WLOCOP stabilizes, suggesting that shrub dominance results in a new, spatially structured connectivity regime.

The FC water WLOCOP in the dry endmember exhibits strong interannual variability, closely tracking rainfall input. Higher rainfall years correspond to longer WLOCOP values, as water moves farther before being absorbed. Under 45% and 60% grazing, WLOCOP tends to be higher than under low grazing, especially during the mid to late simulation years. However, the pattern is not linear, and differences among treatments diminish toward the end of the run, suggesting convergence in network structure regardless of grazing pressure once shrublands are established.

In the wet endmember (Figure S18), WLOCOP trends diverge from those in the dry endmember. For SC water, WLOCOP remains low and relatively stable across all grazing levels, except under 60% grazing, where it rises gradually from 1960, peaks around 1980, and then stabilizes. This delayed and less pronounced increase reflects the slower breakdown of connectivity and later onset of shrub expansion in wetter environments.

For FC water, the WLOCOP shows a more complex relationship with grazing. Unexpectedly, 30% grazing results in the highest mean WLOCOP values, followed by 45%, 60%, and 1 g/m². This ranking remains relatively stable across the time series, suggesting that moderate grazing in wetter systems allows the water to travel farther before interception.

Spatial patterns (see Figure S19) reveal a consistent increase in WLOCOP downslope, particularly as shrubs become dominant. In both dry and wet endmember, WLOCOP values are generally low in upslope areas but increase substantially in the downslope regions during later simulation years, reflecting the spatial concentration of longer flow paths where vegetation sinks are sparse or clustered.

S4.4.2 WL of SC Nitrogen and FC Nitrogen

The mean WLOCOP for SC nitrogen displays considerable interannual variability in both dry and wet endmember (Figure S17 and S18). Across grazing intensities, WLOCOP values are largely comparable, with no consistent pattern differentiating treatments. However, both sites exhibit sharp and irregular peaks during the 1980s to 1990s, particularly under higher grazing pressures. These abrupt fluctuations likely reflect rapid transitions in vegetation structure due to shrub expansion or model sensitivity during regime shifts.

For FC nitrogen, WLOCOP trends differ more distinctly across treatments. In the dry endmember, the lowest WLOCOP values are observed under 60% grazing, while the highest occur under 1 g/m^2 grazing, suggesting that increased grazing shortens nitrogen transport pathways by reducing vegetated sinks. In the wet endmember, the 45% grazing scenario yields the highest WLOCOP, while 60% remains the lowest. Interestingly, 30% and 45% grazing in the wet endmember show similar trajectories, suggesting comparable functional connectivity responses under moderate grazing levels.

The spatial distribution (Figure S20) of WLOCOP for both SC and FC nitrogen follows a downslope gradient, with longer WLOCOP values consistently observed in lower landscape positions. This pattern is consistent with the accumulation of runoff and nutrient movement in the direction of topographic flow, and the increasing distance between vegetated sinks as vegetation becomes more clustered in downslope areas.

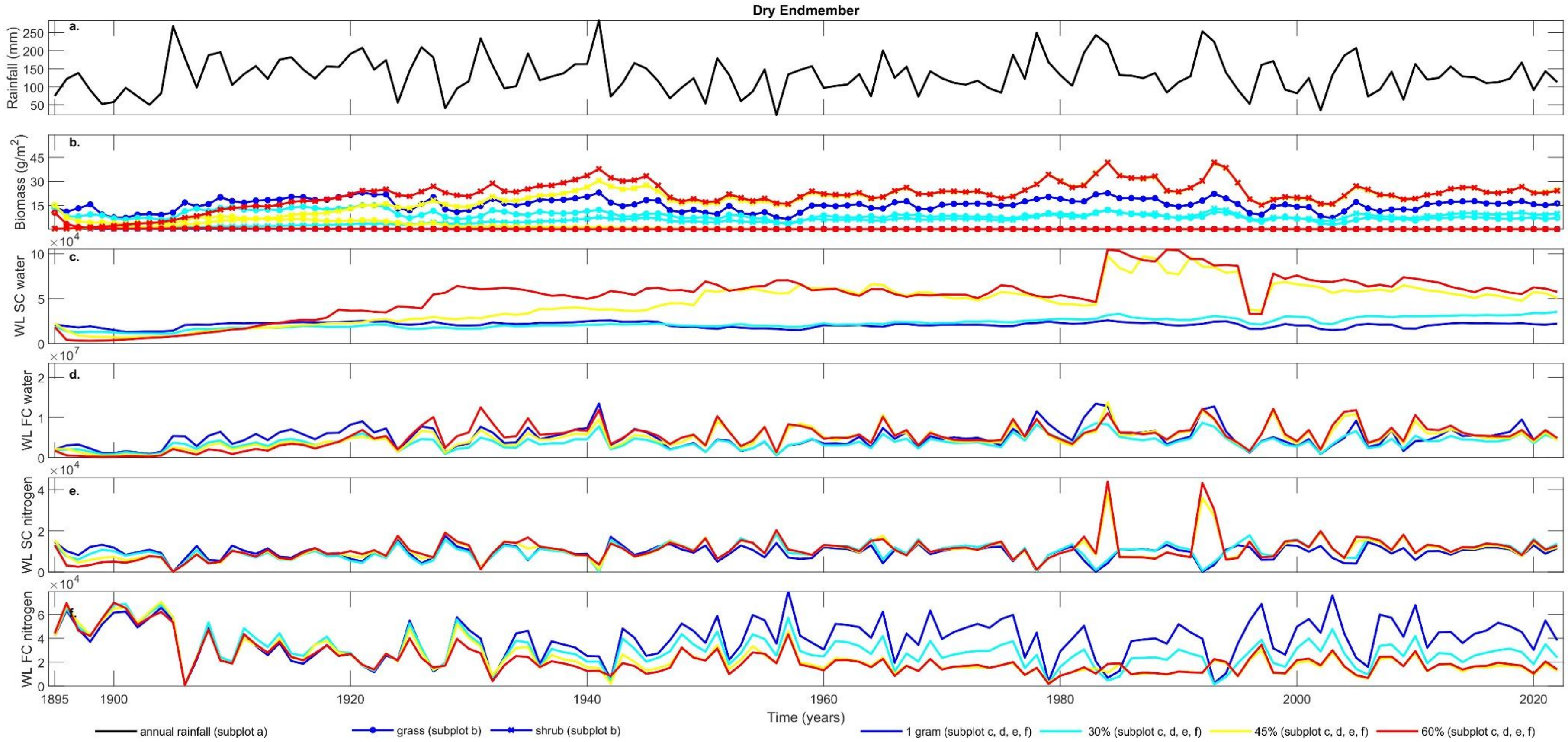

Figure S17. Time series depicting the annual rainfall (mm), mean grass biomass (g/m²), mean shrub biomass (g/m²), and weighted length of connected pathways (WLOCOP) of SC water, FC water, SC nitrogen and FC nitrogen networks for the dry endmember. Data is presented for downslope wind direction and across four grazing intensities: 1 gram, 30%, 45%, and 60%. For figure clarity, WLOCOP is abbreviated as "WL" in axis labels due to space constraints.

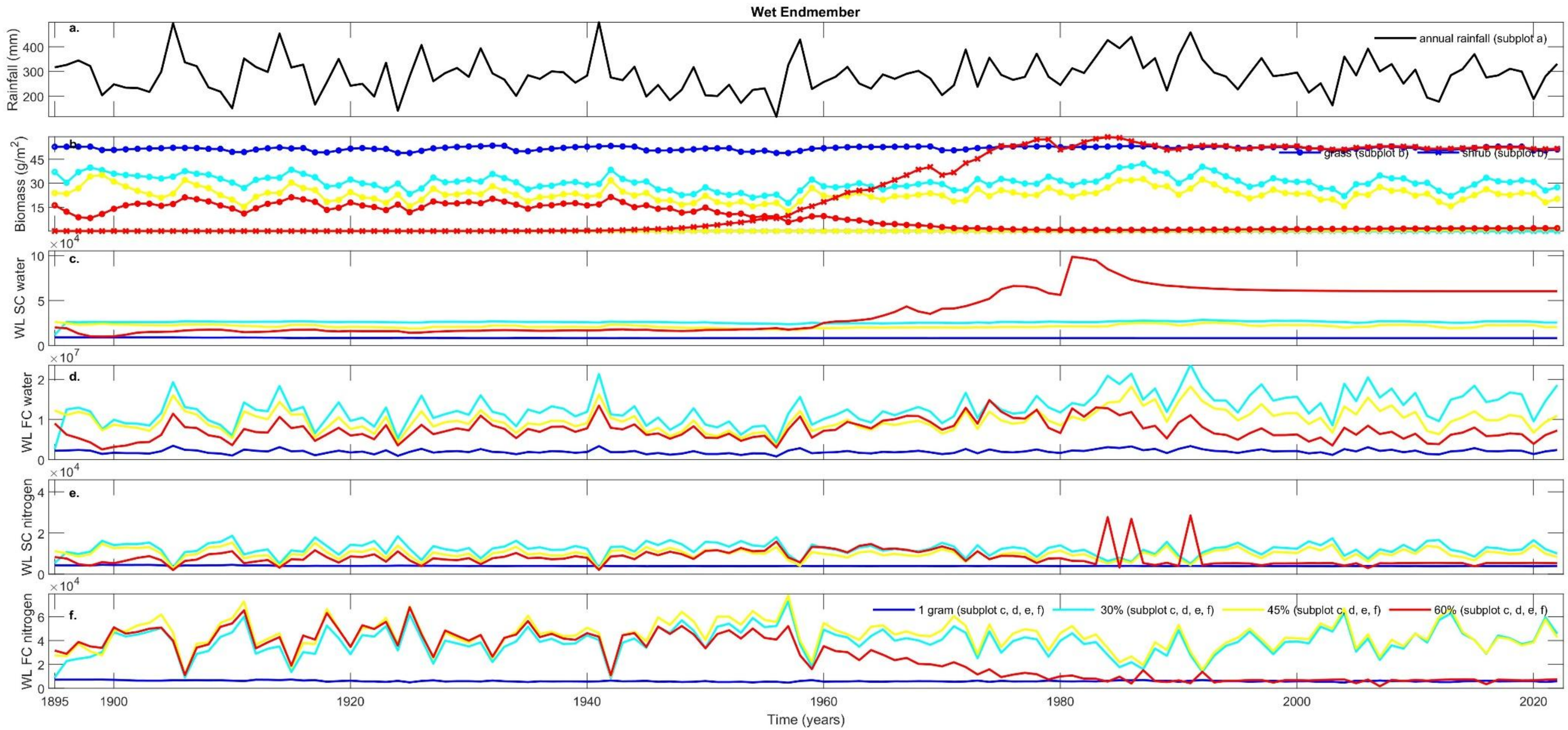

Figure S18. Time series depicting the annual rainfall (mm), mean grass biomass (g/m²), mean shrub biomass (g/m²), and weighted length of connected pathways (WLOCOP) of SC water, FC water, SC nitrogen and FC nitrogen networks for the wet endmember. Data is presented for downslope wind direction and across four grazing intensities: 1 gram, 30%, 45%, and 60%. For figure clarity, WLOCOP is abbreviated as "WL" in axis labels due to space constraints.

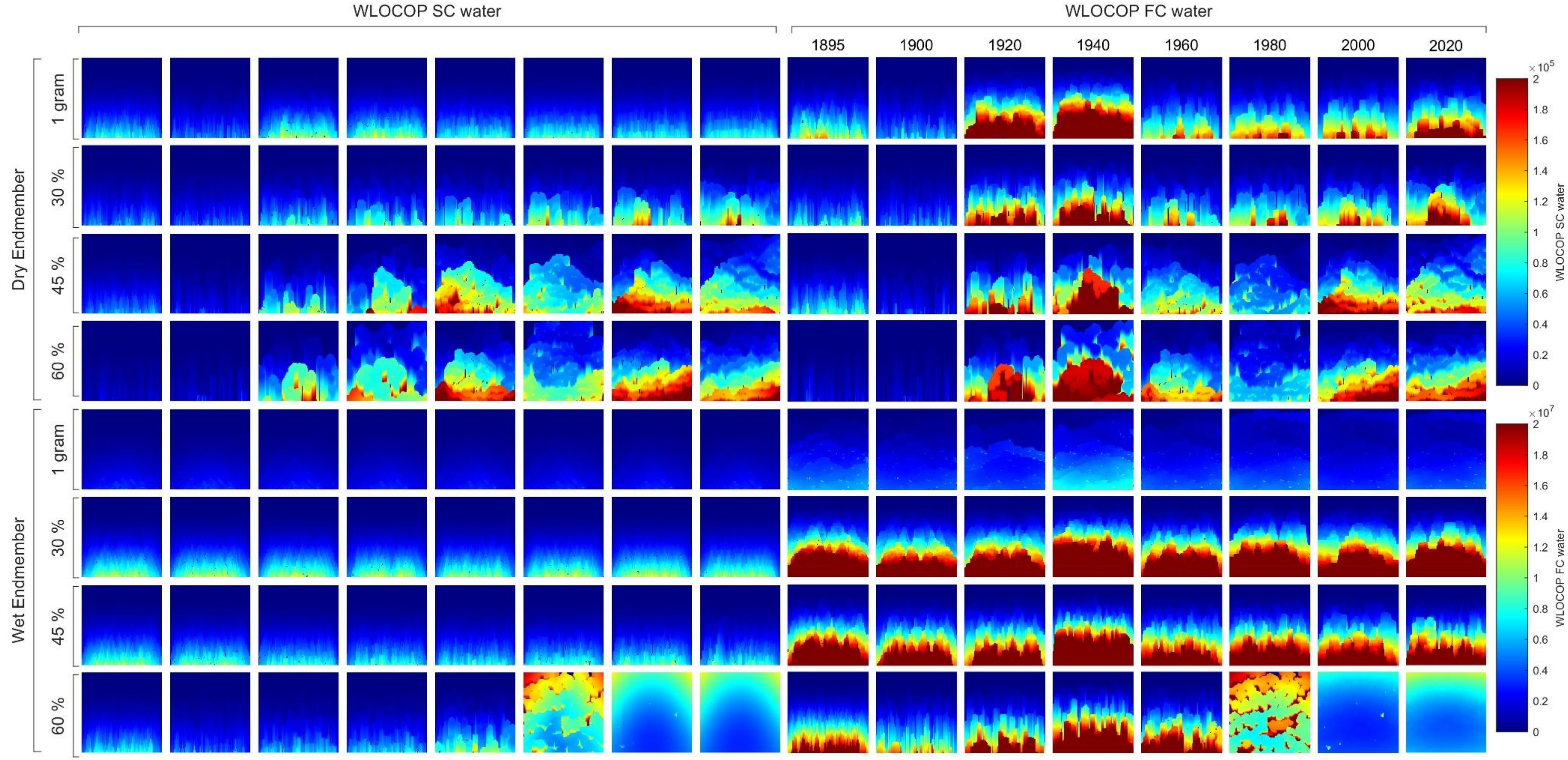

Figure S19. Spatial distribution of Weighted Length of Connected Pathways (WLOCOP) for SC water and FC water network at specific time steps (1895, 1900, 1920, 1940, 1960, 1980, 2000, and 2020) in the dry and wet endmembers. Results are presented for downslope wind directions across four grazing intensities: 1 g/m², 30%, 45%, and 60%.

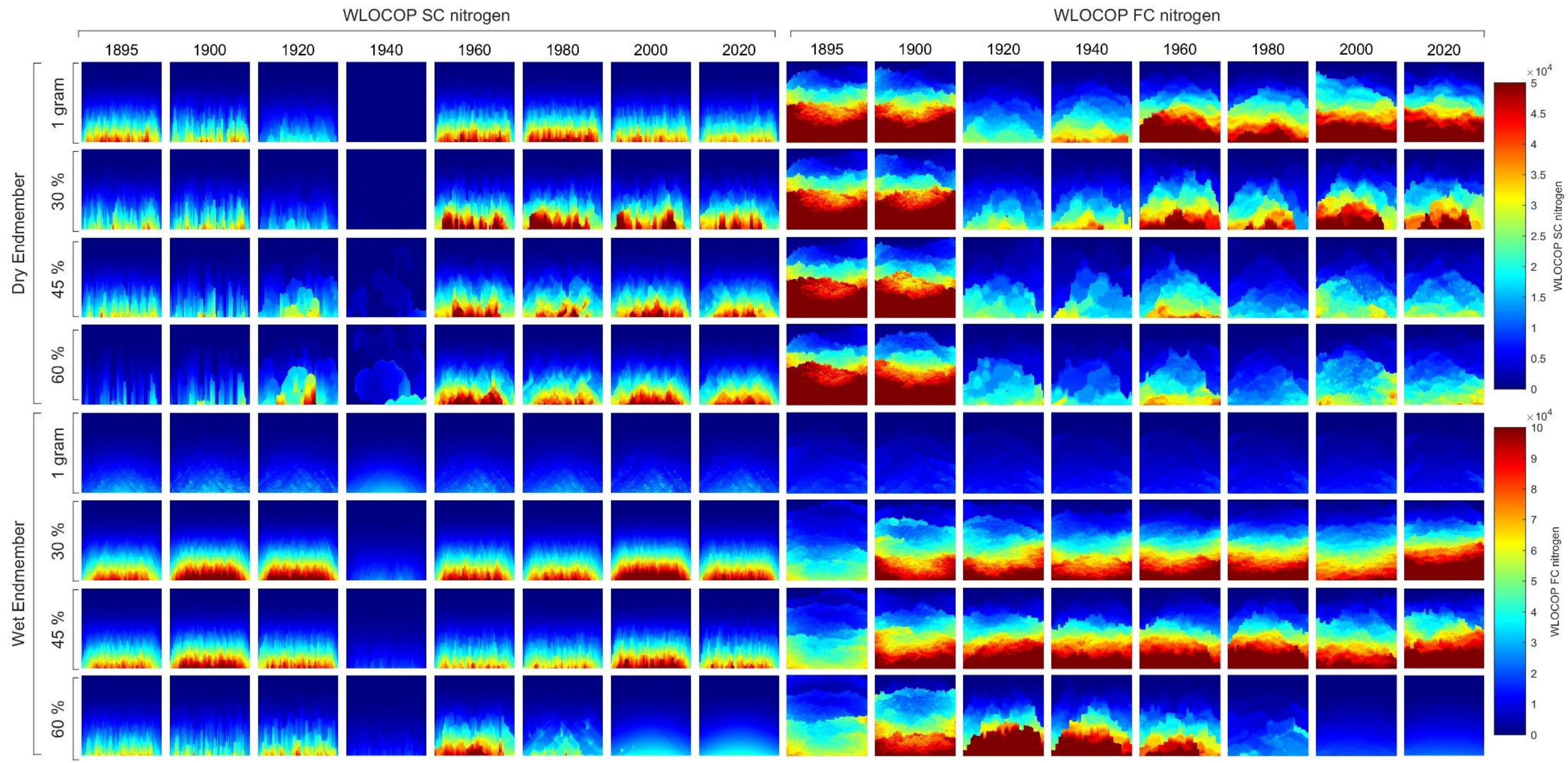

Figure S20. Spatial distribution of Weighted Length of Connected Pathways (WLOCOP) for SC nitrogen and FC nitrogen network at specific time steps (1895, 1900, 1920, 1940, 1960, 1980, 2000, and 2020) in the dry and wet endmembers. Results are presented for downslope wind directions across four grazing intensities: 1 g/m², 30%, 45%, and 60%.

S4.5 Node-Level Early Warning Connectivity Indicators

To evaluate the early warning potential of localized connectivity metrics, we analysed time-lagged correlations between node-level vegetation biomass (grass and shrub) and eight connectivity metrics across all 10,000 grid cells for each year of the simulation (1895–2020). These include betweenness centrality (BC) and weighted length of connected pathways (WLOCOP) for both structural and functional water and nitrogen networks. By computing node-wise correlations at 4-, 8-, and 16-year delays, we capture the spatial and temporal variability of connectivity signals preceding vegetation regime shifts. This analysis complements the node-averaged correlation results presented in the main text (Figure 4), which reflect landscape-scale mean trends.

In the dry climate endmember, under 60% grazing (Figure S24), node-level correlations between shrub biomass and BC SC water and BC FC water increase sharply beginning in the 1950s, peaking between 1970 and 1990. WLOCOP metrics also show moderate and sustained negative correlations with shrub biomass, especially WLOCOP FC nitrogen and WLOCOP SC nitrogen, which show peak correlations around -0.65 to -0.7 during the same period. Grass biomass follows an inverse pattern: BC metrics are initially positively correlated with grass during early decades (1895–1930), but transition to negative correlations from the 1940s onward, particularly at shorter (4-year) lags. WLOCOP SC water shows consistently negative correlations with grass biomass across all delays. These patterns align with BC and WLOCOP time series (Figures S13 and S17), which show connectivity reorganization concurrent with shrub expansion and grass decline.

At lower grazing intensities, early warning signals remain detectable but are less pronounced. Under 45% grazing (Figure S23), shrub biomass shows moderate positive correlations ($r \approx 0.4$-0.6) with BC SC and FC water from 1960 onward, while grass biomass maintains negative correlations during early simulation years. Correlations involving nitrogen networks fluctuate more, reflecting patch-level heterogeneity. WLOCOP metrics show moderately negative correlations with shrub biomass around the 1950-1980 window, strongest at 4-year delays.

Under 30% grazing (Figure S22), correlations with grass biomass dominate the signal. BC FC water and nitrogen metrics are positively correlated with grass during early decades at short lags, while shrub-related signals emerge only weakly after 1980. WLOCOP metrics show some negative correlation with shrub biomass between 1940-1980 but diminish at longer delays.

At 1 g m^{-2} $year^{-1}$ grazing (Figure S21), vegetation remains stable throughout the simulation. Node-level correlations are weak across all metrics and time delays, though BC FC water and nitrogen show weak correlations with grass at 4-year lags during the early years ($r \approx \pm 0.2$). Correlations with shrub biomass are negligible, consistent with the minimal woody encroachment under low disturbance.

In the wet climate endmember, similar patterns are observed, though the signals are more buffered and gradual. Under 60% grazing (Figure S28), strong correlations between shrub biomass and BC SC water and FC water are sustained over multiple decades, with values exceeding r = 0.8 from 1980 onward at both 8- and 12-year delays. WLOCOP SC water shows very strong negative correlations with grass biomass (r ≈ -0.85) at 4-year delays, reinforcing the role of patch fragmentation in functional disconnection. Correlations with nitrogen metrics are weaker overall but maintain consistent direction.

At 45% grazing (Figure S27), grass-related signals are again more prominent. BC FC water and nitrogen show stable, moderate correlations (r ≈ 0.3) with grass biomass during early years, while shrub correlations are weaker and emerge later in the simulation. Similar but weaker patterns are observed at 30% grazing (Figure S26), where functional metrics retain some predictive value for grass but offer limited signals for shrubs. At 1 g m^{-2} $year^{-1}$ (Figure S25), node-level correlations across all metrics are weak and temporally flat.

Across all scenarios, functional metrics (FC) show greater temporal sensitivity, with sharper interannual shifts in correlation direction and magnitude, particularly under intermediate grazing pressures and during periods of rapid structural change (e.g. 1940–1970). In contrast, structural metrics (SC) tend to show smoother, longer-term trends. These node-level results provide spatially explicit evidence of how connectivity reorganization precedes vegetation transitions and offer a more nuanced view than node-averaged results (main manuscript, Figure 4). Temporal trends observed in node-level metrics closely match the connectivity time series presented in Figures S13–S20 and support their role as localized early warning indicators.

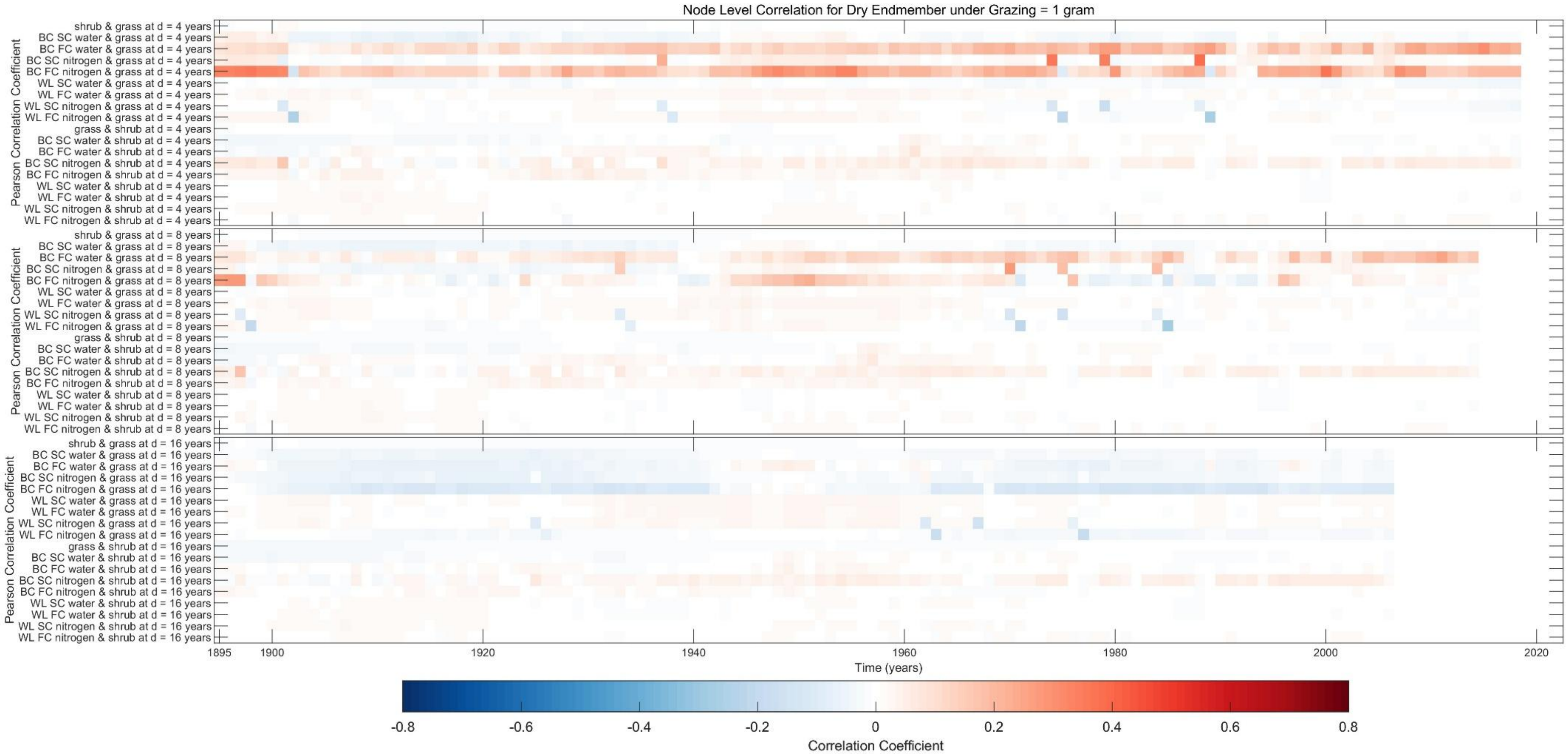

Figure S21. Correlation plots illustrating the relationship between eight node-level connectivity metrics and vegetation biomass (grass and shrub) at the local scale (correlation of 10,000 node metrics for each year). The metrics analysed include BC SC water, BC FC water, BC SC nitrogen, BC FC nitrogen, WLOCOP SC water, WLOCOP FC water, WLOCOP SC nitrogen, and WLOCOP FC nitrogen. Correlations are calculated at time delays of 4, 8, and 16 years to assess the potential of these metrics as early warning indicators of regime shifts. The plots show results for the dry endmember under a grazing intensity of 1 gram and downslope wind direction. For figure clarity, WLOCOP is abbreviated as “WL” in axis labels due to space constraints.

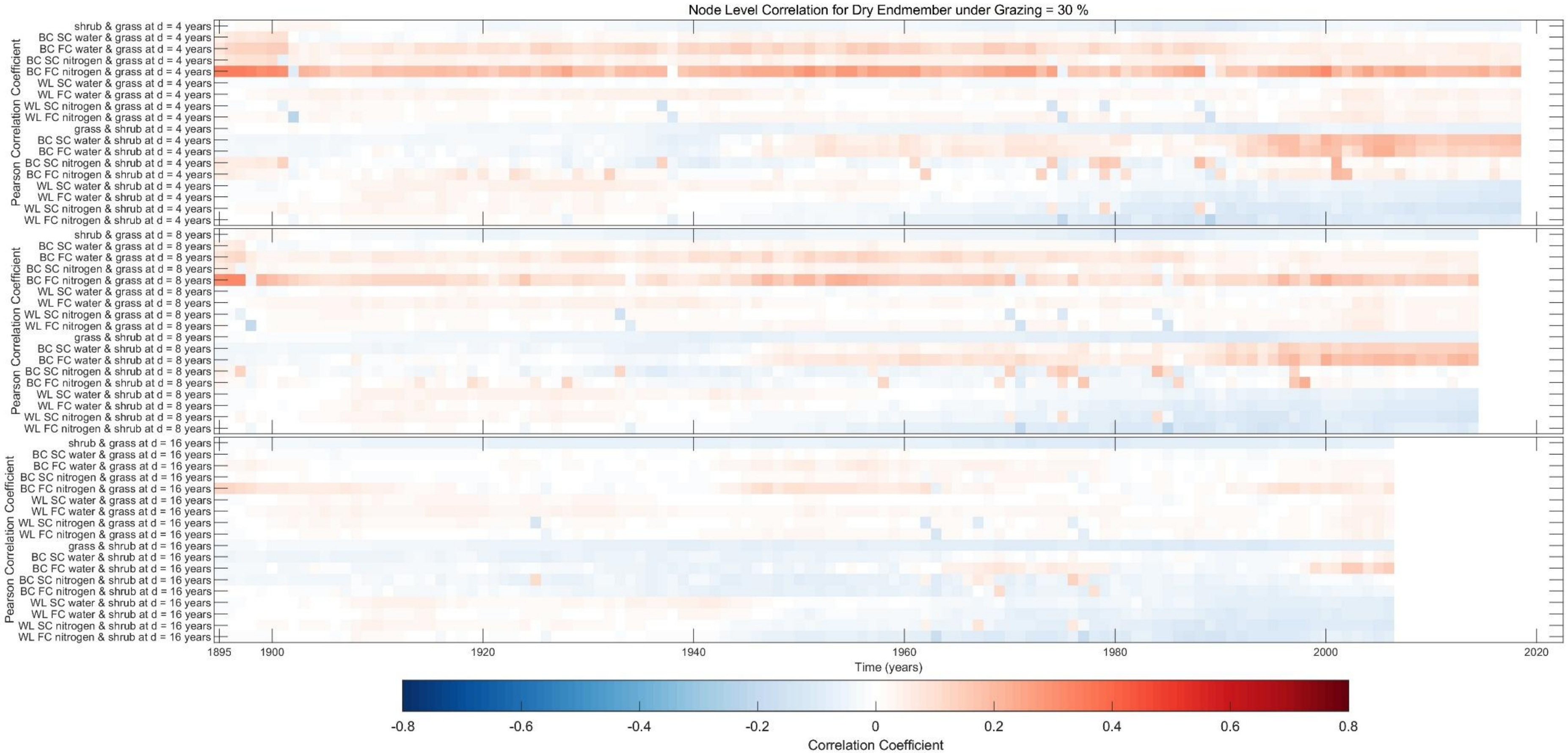

Figure S22. Correlation plots illustrating the relationship between eight node-level connectivity metrics and vegetation biomass (grass and shrub) at the local scale (correlation of 10,000 node metrics for each year). The metrics analysed include BC SC water, BC FC water, BC SC nitrogen, BC FC nitrogen, WLOCOP SC water, WLOCOP FC water, WLOCOP SC nitrogen, and WLOCOP FC nitrogen. Correlations are calculated at time delays of 4, 8, and 16 years to assess the potential of these metrics as early warning indicators of regime shifts. The plots show results for the dry endmember under a grazing intensity of 30 % and downslope wind direction. For figure clarity, WLOCOP is abbreviated as "WL" in axis labels due to space constraints.

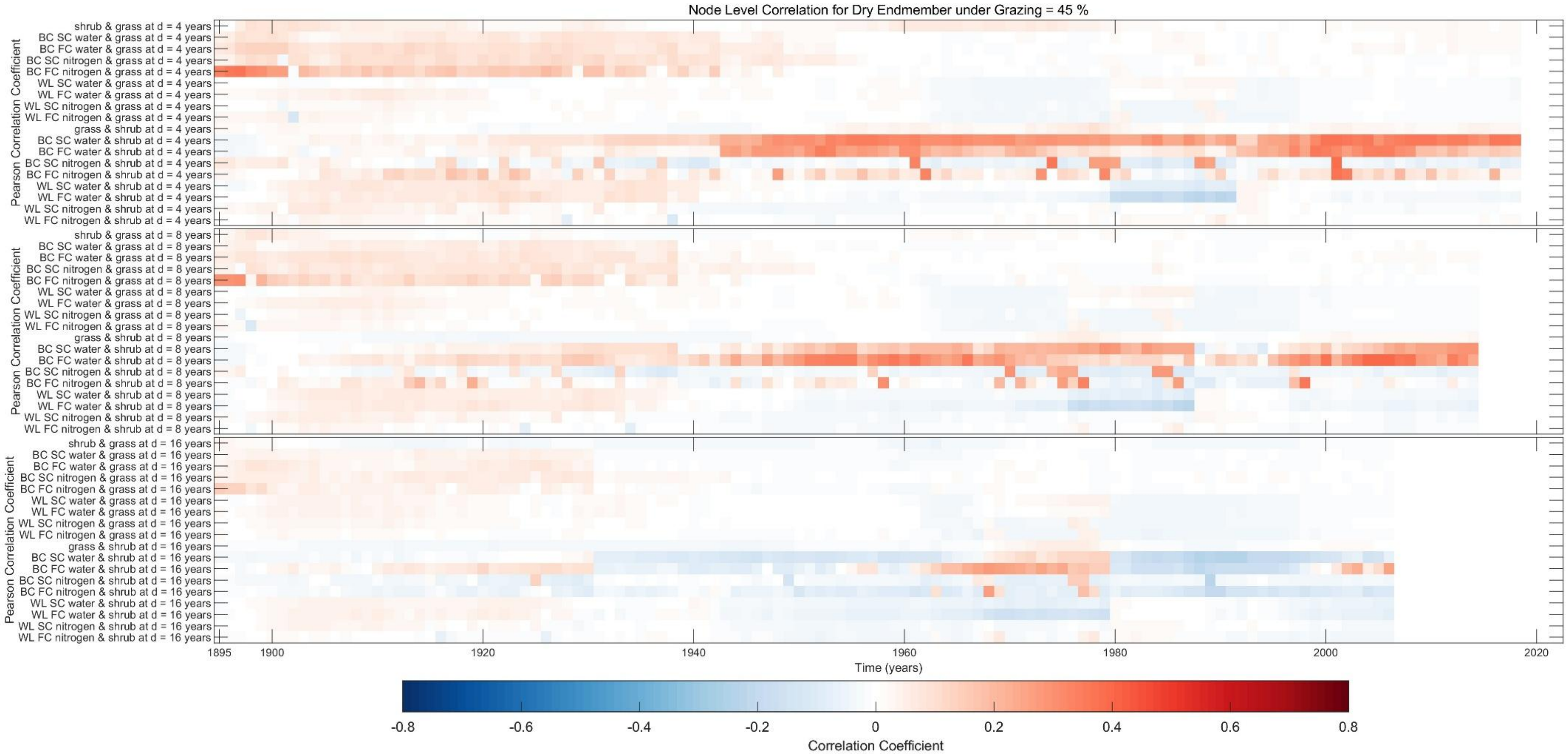

Figure S23. Correlation plots illustrating the relationship between eight node-level connectivity metrics and vegetation biomass (grass and shrub) at the local scale (correlation of 10,000 node metrics for each year). The metrics analysed include BC SC water, BC FC water, BC SC nitrogen, BC FC nitrogen, WLOCOP SC water, WLOCOP FC water, WLOCOP SC nitrogen, and WLOCOP FC nitrogen. Correlations are calculated at time delays of 4, 8, and 16 years to assess the potential of these metrics as early warning indicators of regime shifts. The plots show results for the dry endmember under a grazing intensity of 45 % and downslope wind direction.

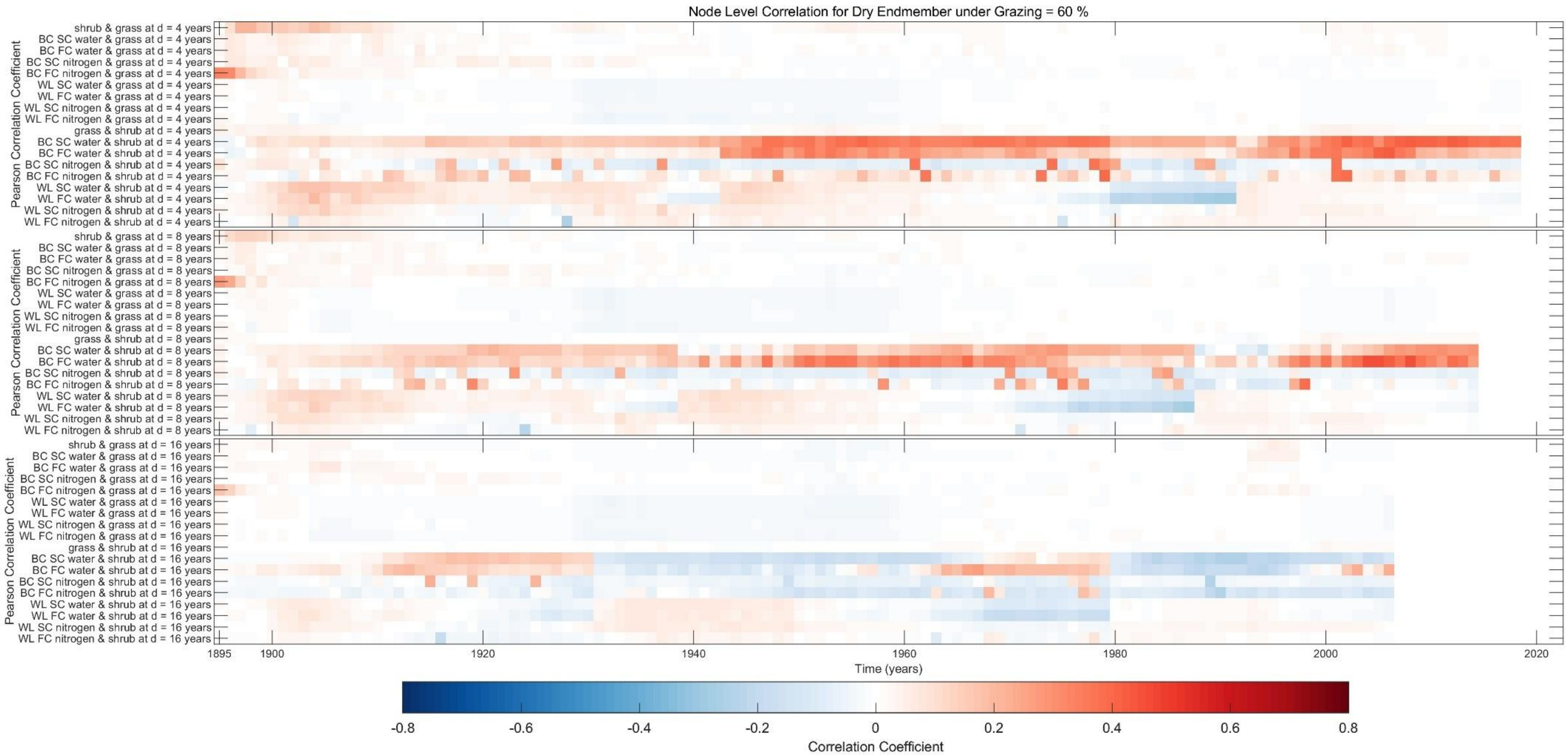

Figure S24. Correlation plots illustrating the relation between eight node-level connectivity metrics and vegetation biomass (grass and shrub) at the local scale (correlation of 10,000 node metrics for each year). Metrics include BC SC water, BC FC water, BC SC nitrogen, BC FC nitrogen, WLOCOP SC water, WLOCOP FC water, WLOCOP SC nitrogen and WLOCOP FC nitrogen. For figure clarity, WLOCOP is abbreviated as "WL" in axis labels due to space constraints. Correlations are calculated at time delays of 4, 8, and 16 years to assess the early warning potential. Results shown are for the dry climate endmember under 60% grazing and downslope wind.

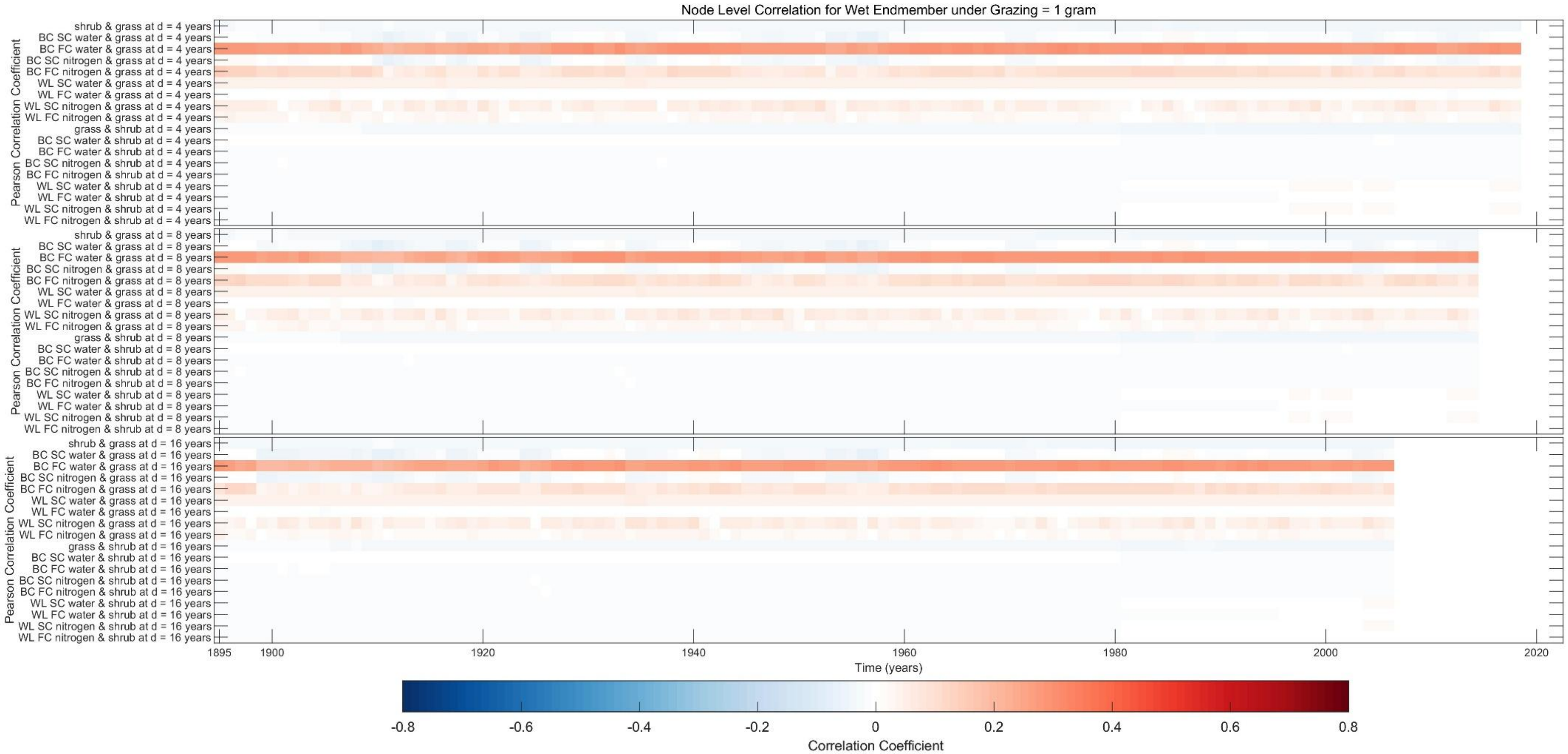

Figure S25. Correlation plots illustrating the relationship between eight node-level connectivity metrics and vegetation biomass (grass and shrub) at the local scale (correlation of 10,000 node metrics for each year). The metrics analysed include BC SC water, BC FC water, BC SC nitrogen, BC FC nitrogen, WLOCOP SC water, WLOCOP FC water, WLOCOP SC nitrogen, and WLOCOP FC nitrogen. Correlations are calculated at time delays of 4, 8, and 16 years to assess the potential of these metrics as early warning indicators of regime shifts. The plots show results for the wet endmember under a grazing intensity of 1 gram and downslope wind direction. For figure clarity, WLOCOP is abbreviated as "WL" in axis labels due to space constraints.

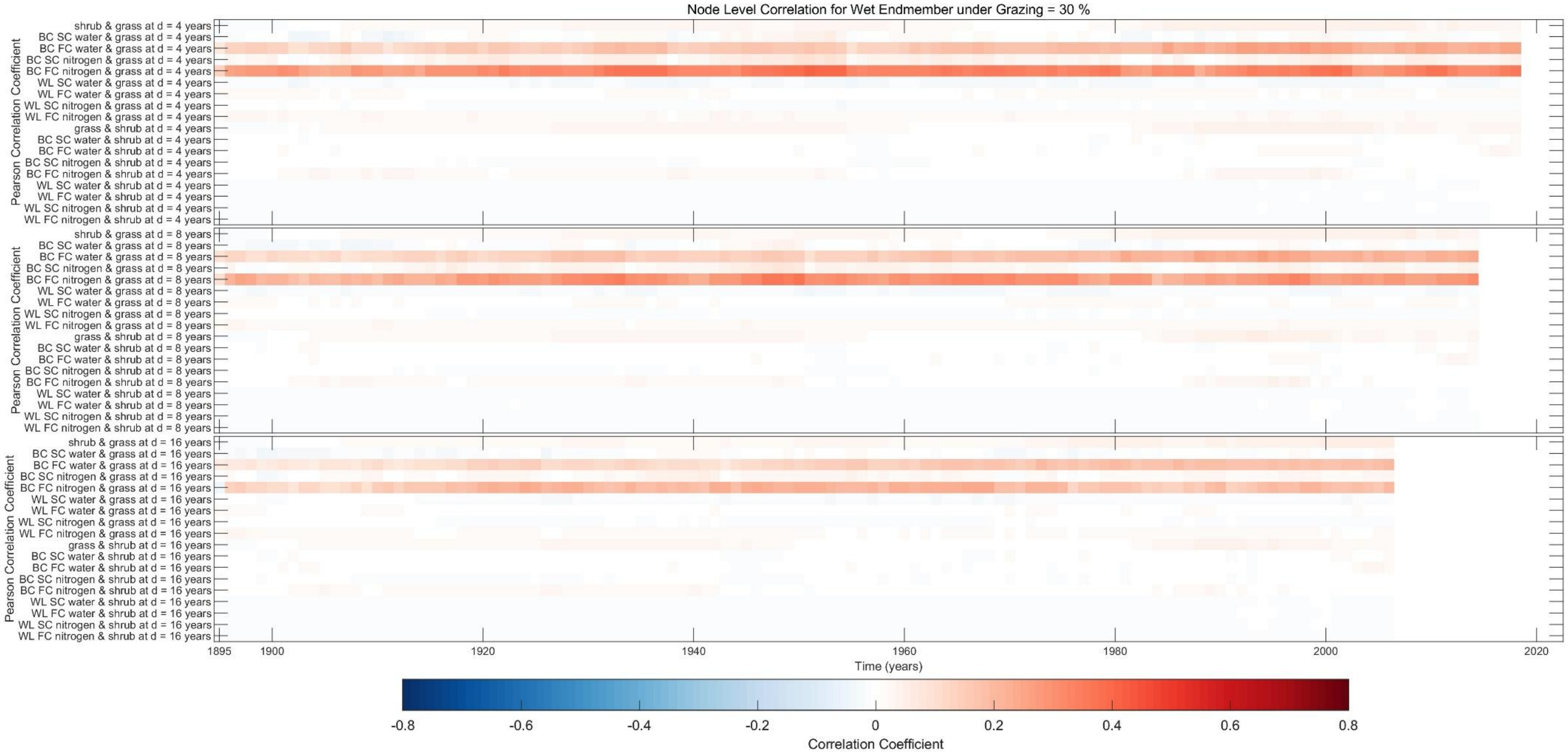

Figure S26. Correlation plots illustrating the relationship between eight node-level connectivity metrics and vegetation biomass (grass and shrub) at the local scale (correlation of 10,000 node metrics for each year). The metrics analysed include BC SC water, BC FC water, BC SC nitrogen, BC FC nitrogen, WLOCOP SC water, WLOCOP FC water, WLOCOP SC nitrogen, and WLOCOP FC nitrogen. Correlations are calculated at time delays of 4, 8, and 16 years to assess the potential of these metrics as early warning indicators of regime shifts. The plots show results for the wet endmember under a grazing intensity of 30 % and downslope wind direction. For figure clarity, WLOCOP is abbreviated as "WL" in axis labels due to space constraints.

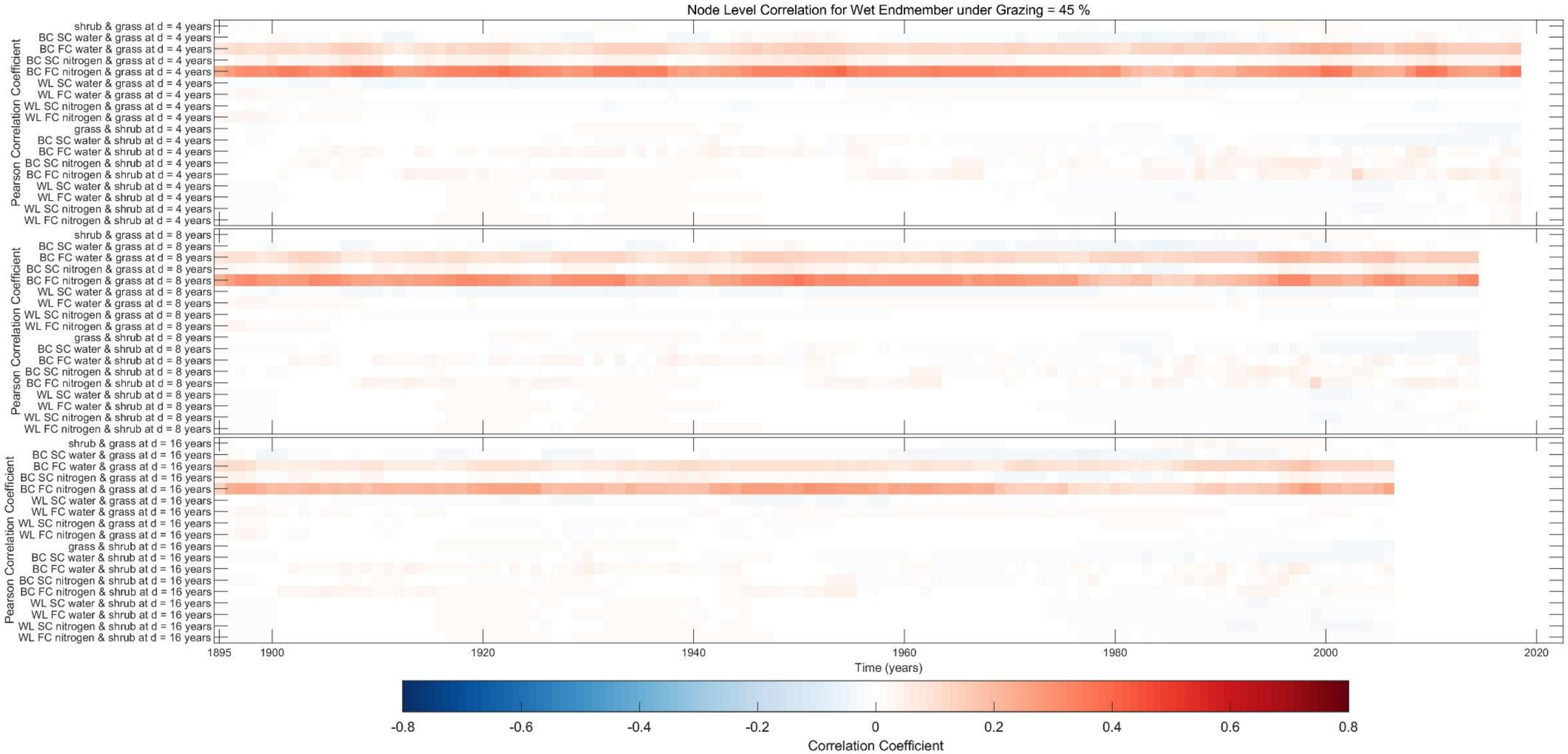

Figure S27. Correlation plots illustrating the relationship between eight node-level connectivity metrics and vegetation biomass (grass and shrub) at the local scale (correlation of 10,000 node metrics for each year). The metrics analysed include BC SC water, BC FC water, BC SC nitrogen, BC FC nitrogen, WLOCOP SC water, WLOCOP FC water, WLOCOP SC nitrogen, and WLOCOP FC nitrogen. Correlations are calculated at time delays of 4, 8, and 16 years to assess the potential of these metrics as early warning indicators of regime shifts. The plots show results for the wet endmember under a grazing intensity of 45 % and downslope wind direction. For figure clarity, WLOCOP is abbreviated as "WL" in axis labels due to space constraints.

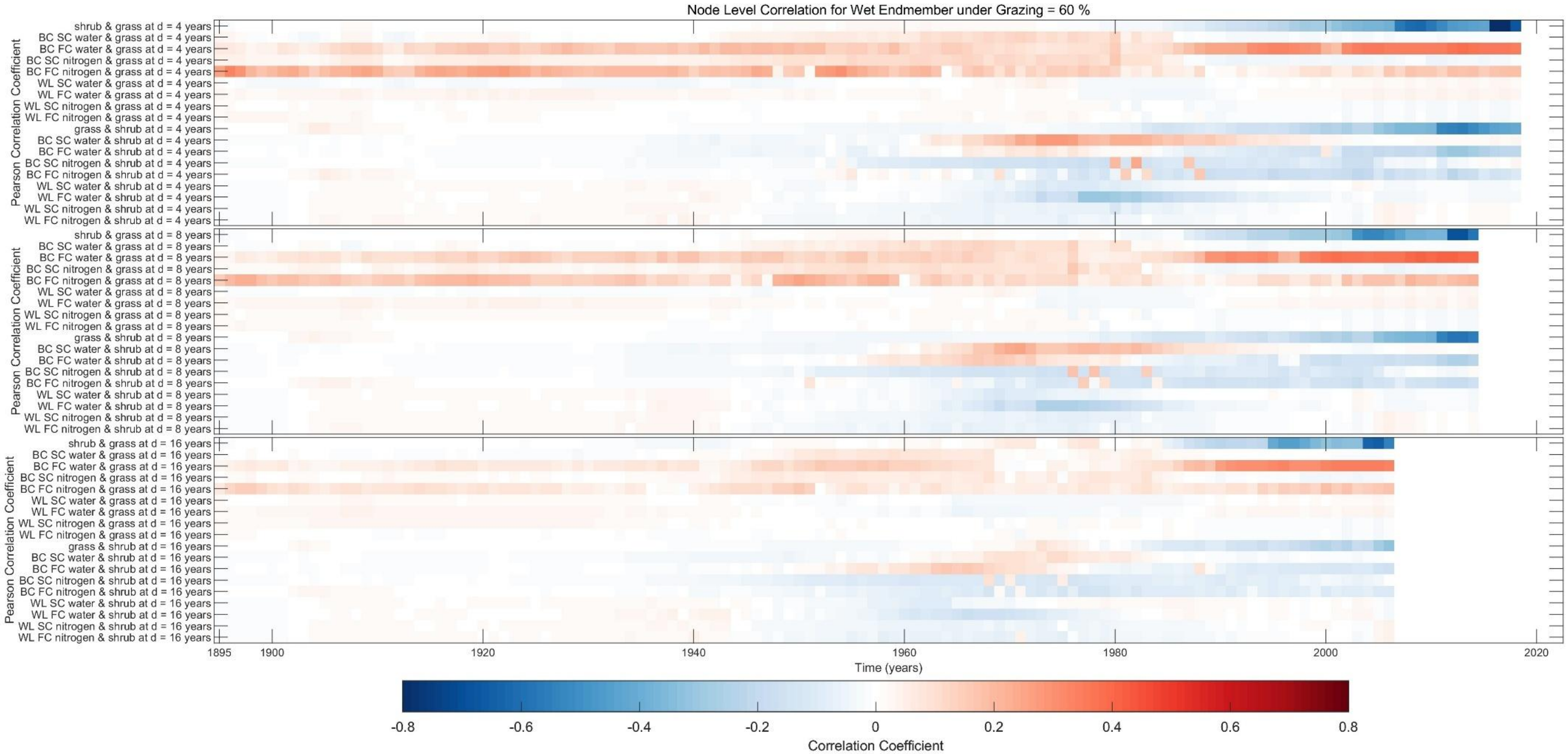

Figure S28. Correlation plots illustrating the relation between eight node-level connectivity metrics and vegetation biomass (grass and shrub) at the local scale (correlation of 10,000 node metrics for each year). Metrics include BC SC water, BC FC water, BC SC nitrogen, BC FC nitrogen, WLOCOP SC water, WLOCOP FC water, WLOCOP SC nitrogen and WLOCOP FC nitrogen. For figure clarity, WLOCOP is abbreviated as “WL” in axis labels due to space constraints. Correlations are calculated at time delays of 4, 8, and 16 years to assess the early warning potential. Results shown are for the wet climate endmember under 60% grazing and downslope wind.

S5 Selected references (full list in main manuscript)

Stewart, J., Parsons, A. J., Wainwright, J., Okin, G. S., Bestelmeyer, B. T., Fredrickson, E. L., & Schlesinger, W. H. (2014). Modeling emergent patterns of dynamic desert ecosystems. *Ecological Monographs*, *84*(3), 373–410. https://doi.org/10.1890/12-1253.1